SANDIA REPORT
SAND2009-6339
Unlimited Release
September 2009

Radiation Microscope for SEE Testing using GeV ions

Gyorgy Vizkelethy, Janelle V. Branson, Khalid Hattar, Barney L. Doyle, Paolo Rossi, David K. Brice, and James A. Knapp

Prepared by
Sandia National Laboratories
Albuquerque, New Mexico 87185 and Livermore, California 94550

Sandia is a multiprogram laboratory operated by Sandia Corporation,
a Lockheed Martin Company, for the United States Department of Energy's
National Nuclear Security Administration under Contract DE-AC04-94AL85000.

Issued by Sandia National Laboratories, operated for the United States Department of Energy by Sandia Corporation.

Available to DOE and DOE contractors from
U.S. Department of Energy
Office of Scientific and Technical Information
P.O. Box 62
Oak Ridge, TN 37831

Telephone: (865) 576-8401
Facsimile: (865) 576-5728
E-Mail: reports@adonis.osti.gov
Online ordering: http://www.osti.gov/bridge

Available to the public from
U.S. Department of Commerce
National Technical Information Service
5285 Port Royal Rd.
Springfield, VA 22161

Telephone: (800) 553-6847
Facsimile: (703) 605-6900
E-Mail: orders@ntis.fedworld.gov
Online order: http://www.ntis.gov/help/ordermethods.asp?loc=7-4-0#online

SAND2009-6339
Unlimited Release
September 2009

Radiation Microscope for SEE testing using GeV Ions

Gyorgy Vizkelethy, Janelle V. Branson, Khalid Hattar, Barney L. Doyle, Paolo Rossi, David K. Brice, and James A. Knapp
01111
Sandia National Laboratories
P.O. Box 5800
Albuquerque, New Mexico 87185-1056

Abstract

Radiation Effects Microscopy is an extremely useful technique in failure analysis of electronic parts used in radiation environment. It also provides much needed support for development of radiation hard components used in spacecraft and nuclear weapons. As the IC manufacturing technology progresses, more and more overlayers are used; therefore, the sensitive region of the part is getting farther and farther from the surface. The thickness of these overlayers is so large today that the traditional microbeams, which are used for REM are unable to reach the sensitive regions. As a result, higher ion beam energies have to be used (> GeV), which are available only at cyclotrons. Since it is extremely complicated to focus these GeV ion beams, a new method has to be developed to perform REM at cyclotrons. We developed a new technique, Ion Photon Emission Microscopy, where instead of focusing the ion beam we use secondary photons emitted from a fluorescence layer on top of the devices being tested to determine the position of the ion hit. By recording this position information in coincidence with an SEE signal we will be able to indentify radiation sensitive regions of modern electronic parts, which will increase the efficiency of radiation hard circuits.

ACKNOWLEDGMENTS

The authors would like to thank Peggy McMahan, Larry W. Phar, and Michael B. Johnson of LBNL for providing beam time for the work and for their continuous support during the experiments at LBNL.

CONTENTS

FIGURES

TABLES

NOMENCLATURE

DOE	Department of Energy
SNL	Sandia National Laboratories
IBL	Ion Beam Laboratory
LBNL	Lawrence Berkeley National Laboratory
IBA	Ion Beam Analysis
IC	Integrated Circuit
SRAM	Static Random Access Memory
REM	Radiation Effects Microscopy
DUT	Device Under Test
LET	Linear Energy Transfer
SEE	Single Event Effects
SEU	Single Event Upset
SET	Single Event Transient
IBIC	Ion Beam Induced Charge/Current
TRIBIC	Time Resolved IBIC
NEM	Nuclear Emission Microscopy
IPEM	Ion-Photon Emission Microscope
PSD	Position Sensitive Detector
MCP	Multi-Channel Plate
COTS	Commercial Off The Shelf
TEM	Transmission Electron Microscope
GaN	Gallium nitride
InGaN	Indium gallium nitride
TBP	Time Between Photons
UV	Ultraviolet
NR	Non radioactive Recombination
IL	Ion Luminescence
IBIL	Ion Beam Induced Luminescence
QW	Quantum Well
PL	Photoluminescence
PMT	Photomultipler Tube
CCD	Charged Coupled Device
GDS	Graphical Design System

1. INTRODUCTION

1.1. Radiation Effects Microscopy

The effect of cosmic and nuclear radiation on electronic devices in satellites, spacecraft, and nuclear weapons has been a problem and is becoming more important with decreasing feature sizes. The radiation induces transient currents in devices, which can eventually lead to the failure of the device. Therefore, in these severe radiation environments special radiation hardened electronic circuits are often used. The design and manufacturing of these radiation-hardened devices require a careful study of the effects of high-energy radiation on them. Furthermore, these devices have to be certified for use in spacecraft, satellites, and nuclear weapons. The usual method to simulate effects of the space and nuclear radiation is the use of high-energy heavy ion beams from particle accelerators. Generally, a device's error rate is measured as a function of the ionizing power of the ion beam. This measurement usually provides two parameters: the threshold LET (Linear Energy Transfer) below which the device is error free and the saturation cross section which gives the probability of failure at very high LETs. In these experiments the whole device is irradiated and the cross section is determined from the number of errors and the ion fluence. Although these broad beam tests provide information about the reliability of the device, they are unable to pinpoint the reason for any specific radiation sensitivity. Device simulations can be used very effectively to determine the sensitive areas of a device [1]. However, since the broad beam tests do not provide the position of the ion strike, it is difficult to directly compare the results to the simulations.

Radiation Effects Microscopy (REM) offers a solution to these problems. In these tests the ion beam can be focused to a submicron spot and scanned over the area of interest [2].The ion strike position is determined by the beam scanning controls, which are only limited to the range that the scanning equipment can cover. From this data, 2D maps can be created using the *x* and *y* position signals recorded in coincidence with the ion-induced signal from the device (which can be either a digital error signal or a current transient on the power supply line). These maps pinpoint the sensitive component of an IC device with micrometer precision. Figure 1 is a schematic of a general REM experiment and Figure 2 shows typical ion beam induced charge (IBIC) and single event upset (SEU) maps for a traditional REM study.

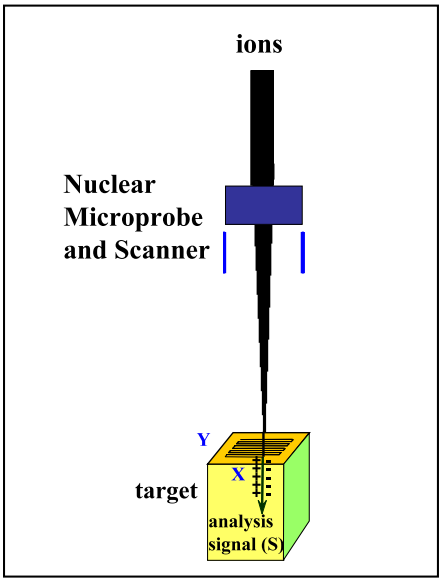

Figure 1 Typical setup of a nuclear microprobe REM experiment

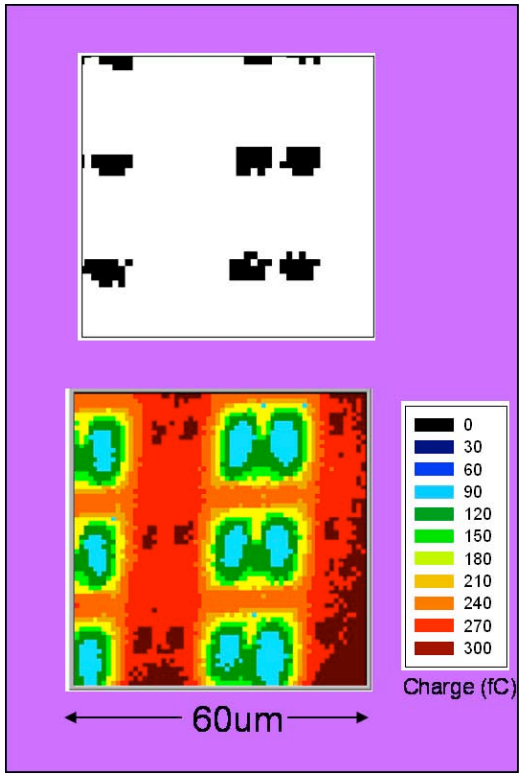

Figure 2 IBIC (bottom color) and SEU (top BW) maps recorded using a microbeam

1.2. Challenges that REM faces in the very near future

Until recently the beam spot of the nuclear microprobes was keeping up with minimum feature size of the ICs as shown in Figure 3.

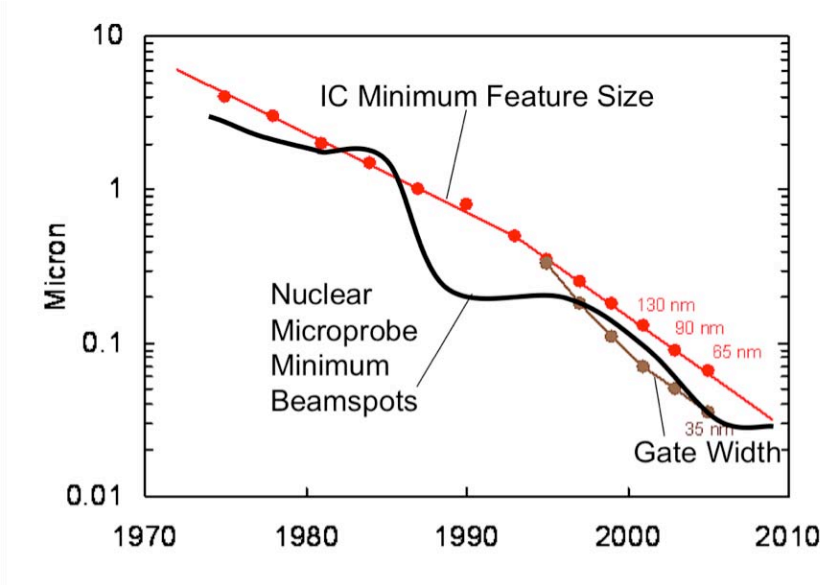

Figure 3 Nuclear microprobe and IC minimum feature sizes

Unfortunately, these microbeams are all proton beams that are used mainly for ion beam analysis or proton beam writing. Proton beams can deliver only a very limited amount of LET (0.5 MeV/(mg/cm^2) @ 55 keV) and as their energy increases, the LET decreases. In contrast, the space radiation consists of high-energy heavy elements with LET up to 100 MeV/(mg/cm^2) as shown in Figure 4. Therefore, we need heavy ions to simulate the space environment successfully.

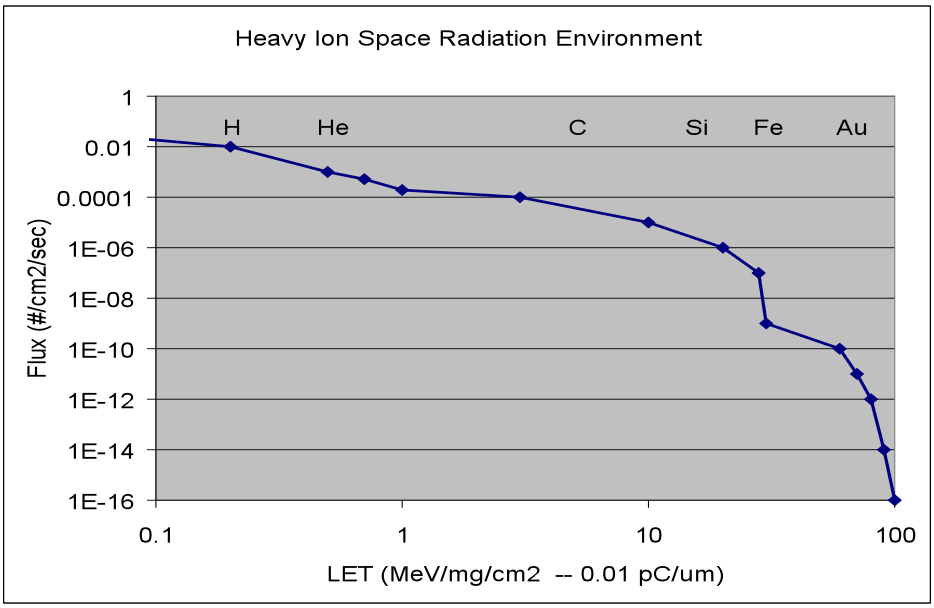

Figure 4 Typical spectrum of the space radiation environment as the function of LET

The second challenge for REM of modern ICs is a result of the increasing overlayer thickness. Modern integrated circuits are characterized by very thick interlevel dielectric and metallization layers on top of the active radiation-sensitive silicon. With these structures, ion beams from tandem accelerators, which can be focused for microprobe applications, no longer have sufficient energy to probe the IC regions of interest. Figure 5 shows the LET of a 50 MeV Cu beam (one of

highest LET for a standard beams used at SNL's IBL) as the function of depth. The square symbols represent the overlayer thicknesses for various SNL technologies.

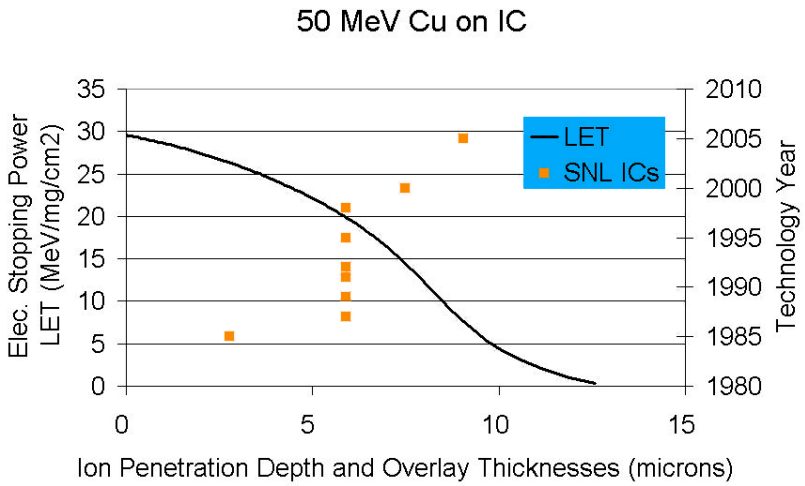

Figure 5 LET of a 50 MeV Cu beam as the function of depth with overlayer thicknesses for various SNL technologies

It is clear from Figure 5 that even for the current generation of SNL ICs the LET of this beam in the sensitive regime is so low that it could not simulate the space radiation environment. To be able to simulate the space environment much higher energy heavy ions is needed and are only available at cyclotron facilities.

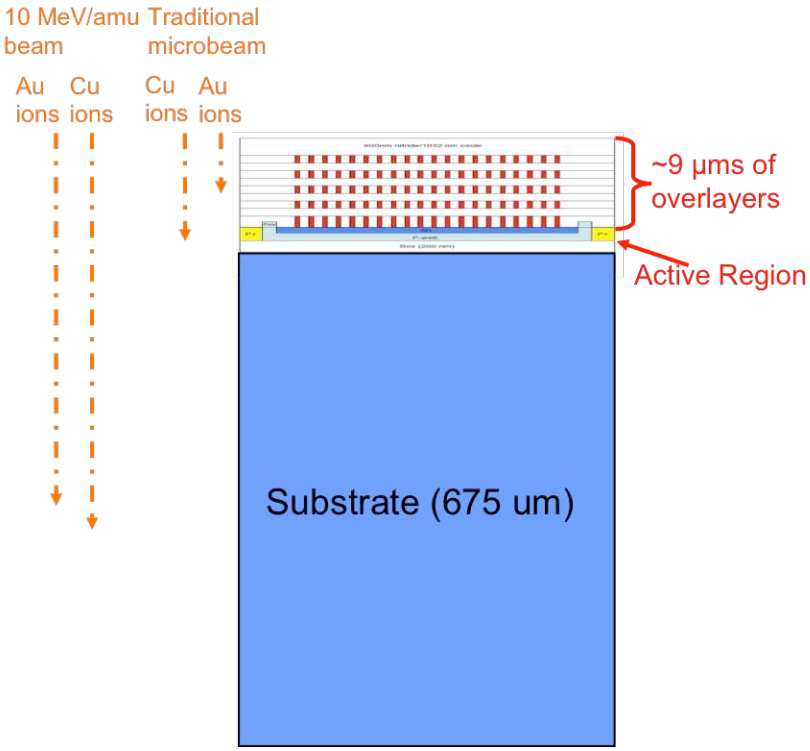

Figure 6 Traditional microbeam and cyclotron ion ranges for a typical modern IC

Figure 6 shows clearly that while the traditional microbeams predominantly range out in 9 μm of overlayer on modern ICs, cyclotron beams (10 MeV/amu is a typical energy for these beams) easily penetrate this overlayer with substantial LET remaining at the sensitive depth. Although cyclotrons have the required energy, it is extremely hard to focus ions from a cyclotron. These ions have high magnetic rigidity, which means that either large magnetic fields are required or long working distances are needed. Both of which will results in less demagnification. In addition, cyclotrons are known for their poor energy resolution, which increases chromatic aberration that leads to a larger disc of confusion. Thirdly, due to their extreme high energy, these ions will have much larger slit scattering (due to interactions with the blade edges of the slits) further increasing the spot size. Currently, there is one cyclotron-based focused ion microbeam at the Takasaki institute of the Japan Atomic Energy Agency [3, 4]. The development of that focused ion microscope required a huge financial and scientific effort and mainly applied to biological specimens. A final concern is that many radiation effects test should be carried out in air since they might require complicated circuit boards that either do not fit into a vacuum chamber or cannot be operated in vacuum.

An alternate way to focus the ions is an ion microscope that is tailored after a traditional optical microscope, which uses a floodlight to illuminate the specimen and focusing lenses to image the sample. Similarly, if we can find secondary particles that are emitted due to ion bombardment and we can focus and image these particles, then by recording these position signals in coincidence with and IBIC or SEE signal, we can build IBIC and SEE maps, just as was done with the focused ion beam in classical REM.

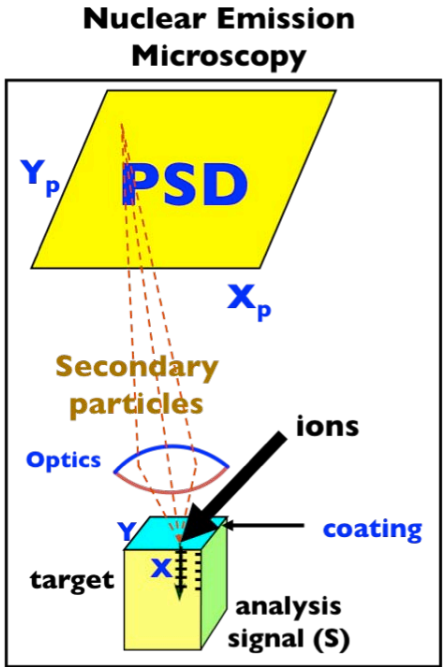

Figure 7 General schematics of Nuclear Emission Microscopy

Figure 7 demonstrates the general principle of such a system, called Nuclear Emission Microscopy (NEM) [5]. The unfocused ion beam hits the DUT (secondary particle-producing coating on the DUT), and the secondary particles (electrons or photons) are focused through some optics

and imaged onto a position sensitive detector, which produces an *x* and *y* signal. This signal recorded in coincidence with electronic signal from the DUT will create the required SEE maps. One system was developed at SNL using secondary electrons and an electron microscope, called the Ion Electron Emission microscope (IEEM). This system was installed on the SNL tandem-RFQ combined system where 380 MeV Au beam could be used for SEE testing [6-8]. The system was difficult to use and will never work in air. Nonetheless, a similar system is being developed at INFN in Legnaro, Italy [9-13].

A different approach designed and developed at SNL uses photons as secondary particles. This method, which is called Ion Photon Emission Microscopy (IPEM), is described in the next sections.

2. THE PRINCIPLE OF THE IPEM

Ion luminescence (IL) is a known phenomenon in nature that has already been harnessed for a materials analysis technique called Ion Beam Induced Luminescence (IBIL). In this phenomenon, accelerated ions interact with a solid, the atoms are subsequently ionized or in a semiconductor, electrons are raised into the conduction band. In a certain group of materials these excited atoms return to their ground state (or electrons to the valence band) through a radiative process by emitting photons. These photons are emitted randomly obeying the Poisson statistic with a characteristic lifetime. Most of these photons leave the solid and then can be focused and imaged to determine where the ions hit. If the IL solid is thin enough, the resulting light will appear to have come from the impact point of the ions on the surface and ions can continue into the DUT. We can convert a general NEM, Figure 7, to IPEM, Figure 8, by the addition of traditional light optics and a single photon PSD. A single photon PSD usually consists of a layer that converts the photons to electrons, an MCP that creates an electron cascade, and a resistive anode that allows the determination of the position of the photon hit. The conversion layer is in most cases some bi-alkali or multi-alkali material. The signals from the four corners of the PSD are fed into a position analyzer that produces pairs of signals that are proportional to the *x* and *y* positions of the photon impact. These analog signals are then processed by a multi-parameter data acquisition system in coincidence with a signal from the DUT. This signal can be either a current transient (IBIC, TRIBIC, SET) or an error signal as in case of SEU mapping. Generally, the data are recorded in list files for later processing but today's multiparameter data acquisition systems permits the generation of real time maps.

Although the idea seems very simple, the realization of an IPEM system is quite complicated. There are several requirements for the luminescent film that provides the position information:

- The film has to be thin enough that
  - the ions do not lose significant energy within the film,
  - the energy spread is small enough not to smear out IBIC measurements,
  - the difference between the entry point (which we image) and the exit point (where the interaction with the DUT occurs) of the film is small enough, as not to significantly affect spatial resolution, and
  - to have minimal effect from blooming[1].
- The overall efficiency of photon detection has to be around one. Less efficiency would mean there would be signals from the DUT when no position information is received. It would lead to both longer test times and increased damage to the DUT. Much higher efficiency would cause problems with precise position determination and would overdrive the detection system. This detection efficiency has several components:
  - the luminescence efficiency of the film,
  - the transmission efficiency of the optical system, and
  - the detection efficiency of the PSD.

[1] The photons originating from different depths exit the foil at some distance from the impact point and the image appears as a circle rather than a point.

- The film should have high resistance to radiation damage, i.e. its luminescence yield should not change significantly with the irradiation fluence to be able to use it for several tests.
- The wavelength of the emitted light should be in the detection range of the PSD.
- The lifetime should be short enough to allow reasonable ion rate in the order of 100-1000 ions/s.

In addition, it is desirable to be able to

- Correlate the optical image with the SEE map,
- Navigate on the DUT based on optical images or GDS II design layout files.

The properties of different luminescence films investigated will be discussed in Section 4, the life time measurements theory will be given in Section 3, and hardware and software considerations will be presented in Section 5.

To demonstrate the proof of principle, a tabletop IPEM using a Po-210 alpha source and a PSD mounted on an ordinary optical microscope was built. This system would not fulfill the requirements for testing modern ICs; the alpha particles had only the energy of about 5 MeV. But in addition to providing proof-of-principle equipment, it has some potential to be used in testing COTS parts that are much more sensitive. The tabletop setup can be placed at the end of a production line and quickly provide quality assurance of radiation hardness for individual chips.

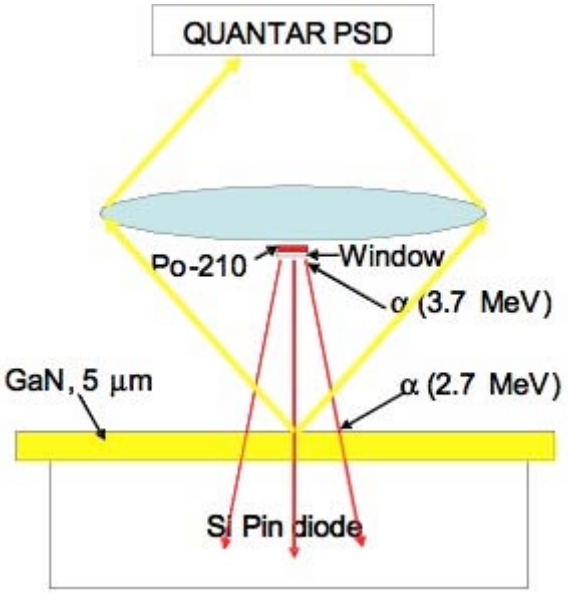

Figure 8 The schematic setup of the tabletop IPEM

Figure 9 Photograph of the tabletop IPEM

Figure 8 is a schematic of the tabletop IPEM and Figure 9 is an image of the equipment. Experiments with the tabletop IPEM not only proved the concept, but also allowed some preliminary resolution measurements.

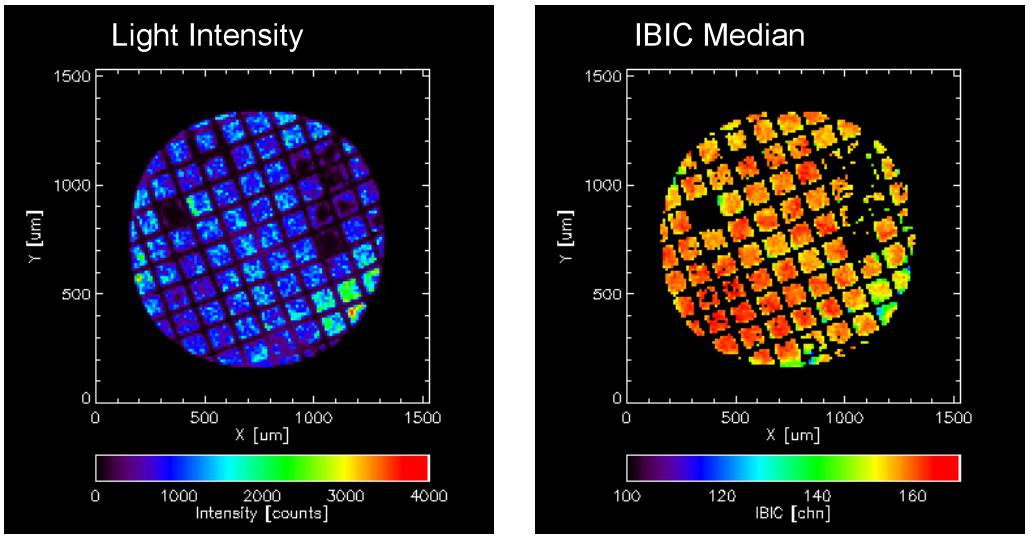

Figure 10 Intensity and IBIC median maps of a TEM grid recorded with the tabletop IPEM.

Figure 10 shows intensity and IBIC median maps of a TEM grid placed on top of the luminescent film on top of a PIN diode. Here the intensity and the IBIC median maps are very similar. Since the grid was on top of the luminescent film, there were no photons generated when the ions hit the wire in the grid. Similarly, no IBIC signal was produced in these cases since the ions stopped in the GaN film and did not reach the PIN diode. This proof-of-principle experiment showed that with this simple setup a resolution about 5 μm could be achived.

3. THE THEORY OF THE TIME BETWEEN PHOTONS [14]

To measure lifetime of luminescent materials we need to know how the number of detected photons affect the time between photons. Phosphors emit light in different modes that depend on the exciting radiation, so that one speaks of photo-, cathode- or ion- luminescence. The usual way to measure the lifetime of phosphor's excited centers is to shine them with an intense short pulse of the radiation of interest and then measure the emitted light intensity as a function of time. The substantial power released to the phosphor might sometimes modify the material and give unpredictable results. We propose here an alternate way to measure the phosphor's lifetime that employs an extremely low exciting current and actually applies only to ion-luminescence. We have to disentangle the photons (up to several thousand) generated by a single ion and employ a single-photon detector able to measure the photon arriving time with high timing resolution. The TBP theory described here is able to connect this "arrival time" to the phosphor lifetime, which is what we want to know.

The theory concerns the detection of photons emitted from a phosphor that is traversed by a single ionizing particle. N is the number of excited atoms that decay radiatively, i.e. emitting photons. N may range up to a few thousand for each ion. The photons, emitted isotropically, are detected according to an efficiency S that is a small fraction of 1, like 10^{-2} to 10^{-5}. Moreover, the detector has a dead time, typically a few hundreds of nanoseconds, which usually prevents, in case of fast phosphors (e.g. light emission of plastic scintillators) the detection of all the photons. Some detectors, such as photo-converters coupled to microchannel plates, are capable of detecting single photons, and we call the initial ion-induced photon detected "the first detected photon". If the phosphor is slow, e.g. emitting light for microseconds or even hundreds of microseconds after excitation, one may be also measure the detection time of the second, third, … photons and thereby determine the "time between two consecutive detected photons". The TBP theory offers a functional connection between the probability distributions of these two experimentally measurable quantities, i.e. the "first detected photon time" and "the time between detected photons", to the lifetime of the phosphor.

We restrict ourselves to a basically simple situation, where the phosphor material is homogenous, the individual decays are independent from each other and the excited atoms, no matter how long they were in the excited state, have the same probability of decay. Of course, if the concentration is high enough, there might be stimulated emission, i.e. a laser-like effect, or, if the excited states are sufficiently extended to allow overlap of the wave functions, there might be cooperative effects. But we here disregard these complex situations.

The "simple situation" we defined above is formally equivalent to the decay of radioactive isotopes in nuclear physics and may be treated in the same way. Of course, we handle here "only" thousands (N) of excited atoms (those corresponding to a single ion). The number of detected photons may range from nearly zero to a few units, and the time between detected photons may be large enough to be measured. Going back to the nuclear decay analogy, we postulate that the relative increment, during the interval dt, of the probability $P_L(t)$ for the atom to be still in an excited state is proportional to dt according to the differential equation:

$$\frac{dP_L(t)}{P_L(t)} = -\frac{dt}{\tau} \qquad (3.1),$$

where τ is a positive constant. The subscript "*L*" of $P_L(t)$ indicates that an atom is still "Living" in its excited state at the time *t*. The well known solution, with the condition that the initial probability $P_L(t=0) = 1$, is $P_L(t)=e^{-t/\tau}$. Also, the probability that an atom decays in the time interval *[0,t]*, is $P_D(t) = 1-e^{-t/\tau}$, or the differential probability that an atom decays in the interval *[t, t+dt]* is $dP_D(t) = dt\,(1/\tau)\,e^{-t/\tau}$, which is simply the analog of the differential "activity" in nuclear physics.

What is the differential probability $dP_D^{(1)}$ that the "first" decay happens in *[t, t+dt]*? For each atom, it is simply the product of the probability to decay and the probability that all the other atoms are still alive. Then we have to sum over all atoms, i.e. simply multiply by *N*.

$$dP_D^{(1)} = N \cdot dP_D(t) \cdot P_L(t)^{N-1} = N \cdot \frac{e^{-\frac{t}{\tau}}}{\tau} \cdot \left(e^{-\frac{t}{\tau}}\right)^{N-1} dt = \frac{1}{\tau \cdot N} e^{-\frac{t}{\tau \cdot N}} \qquad (3.2).$$

So, the probability for the "first" photon to be emitted is similar to the probability of a "generic" photon to be emitted; only τ has to be replaced by τ/N.

If *S* is the detection efficiency, the probability that a photon is detected in *[0,t]* is $P_S(t) = S\,P_D(t) = S\,(1 - e^{-t/\tau})$, or is detected in *[t, t+dt]* is $dP_S(t) = dt\,(1/\tau)\,S\,e^{-t/\tau}$; while the probability of being undetected in *[0, t]* is: $P_U(t) = 1-P_S(t) = 1-S+S\,e^{-t/\tau} = U+S\,e^{-t/\tau}$.

The probability $dQ_D^{(1)}$ of the "first" detected decay in *[t, t+dt]* is, for each atom, equal to the probability that its emitted photon is detected in *[t, t+dt]* multiplied by the probability that the others *N-1* atoms decays are being undetected in *[0,t]*. Then, one has to sum up over all atoms: And if $U = 1- S$, then:

$$dQ_D^{(1)} = N \cdot P_U(t)^{N-1} \cdot dP_S(t) = \frac{N \cdot S}{\tau} e^{-\frac{t}{\tau}} \cdot \left(U + S \cdot e^{-\frac{t}{\tau}}\right)^{N-1} \cdot dt \qquad (3.3).$$

It should be noted that if $S<<1$ (so $U\sim1$), the last formula becomes simply $dQ_D^{(1)} : \frac{N \cdot S}{\tau} e^{-\frac{t}{\tau}} dt$, and the 1st detected decay time distribution is a simple exponential with τ as time constant. This suggests a method to measure τ: measure the distribution of 1st photon detection times and determine the average number of detected photons (*NS*).

The probability $dQ_D^{(k)}$ that the "k^{th}" decay occurs in *[t, t+dt]* is, for each atom, equal to the probability that its photon is detected multiplied by the probability that *k-1* atoms have already been detected and *N-k* have not been detected. Then, one has to multiply the result by the combinatorial factor that gives the number of ways in which this may happen which is: $k \cdot B(N,k) = \frac{k \cdot N!}{k! \cdot (N-k)!}$, or combining:

$$dQ_D^{(k)} = k \cdot B(N,k) \cdot P_S(t)^{k-1} \cdot P_U(t)^{N-k} \cdot dP_S(t) \qquad (3.4).$$

Now

$$P_U(t)^{N-k} = \left(U \cdot P_D(t) + P_L(t)\right)^{N-k} = \sum_{m=0}^{N-k} B(N-k,m) \cdot \left(U \cdot P_D(t)\right)^{N-k-m} \cdot P_L(t)^m \qquad (3.5),$$

hence:

$$dQ_D^{(k)} = \frac{k \cdot B(N,k) \cdot e^{-\frac{t}{\tau}} \cdot S^k \left(1 - e^{-\frac{t}{\tau}}\right)^{k-1}}{\tau} \sum_{m=0}^{N-k} B(N-k,m) \cdot \left(U \cdot P_D(t)\right)^{N-k-m} \cdot P_L(t)^m \cdot dt \quad (3.6).$$

The factors in the sum represent:

1. $UP_D(t)^{N-k-m}$, the probability that *N-k-m* atoms have decayed but stayed undetected.
2. $P_L(t)^m$, the probability that m atoms stay excited.
3. *B* is the combinatorial coefficient.

If *m* atoms are excited at *t*, the probability that the first detected decay of this group occurs in *[t+T, t+T+dT]* is

$$dQ_D^{(1)}(m,T) = \frac{\tau}{m} \cdot S \cdot e^{-\frac{T}{\tau}} \cdot \left(U + S \cdot e^{-\frac{T}{\tau}}\right)^{m-1} \cdot dT \qquad (3.7),$$

hence multiplying each term $P_L(t)^m$, representing the probability that *m* atoms stay excited, inside the sum in (3.6) by $dQ_D^1(m,T)$, we obtain the probability, $d^2R_D^{(k+1)}(t,T)$, that the k^{th} detected photon is observed in *[t,t + dt]* and the $(k + 1)^{th}$ detected photon follows in *[t + T, t + T + dT]* is:

$$d^2R_D^{(k+1)}(t,T) = \frac{k \cdot B(N,k) \cdot e^{-\frac{t}{\tau}} \cdot S^k \cdot \left(1 - e^{-\frac{t}{\tau}}\right)^{k-1}}{\tau} \cdot dt \cdot \sum_{m=0}^{N-k} \left[B(N-k,m) \cdot \left(U \cdot P_D(t)\right)^{N-k-m} \cdot P_L(t)^m \cdot dQ_D^{(1)}(m,T) \right] \quad (3.8).$$

Evaluating the sum and integrating this expression over *t* from 0 to ∞, with a complex procedure that we do not report here, we obtain that the probability $dR_D^{k+1}(t,T)$ that the time between the *k* and *k+1* photon measured in the time interval *[T,T + dT]* is simply:

$$dR_D^{k+1} = \frac{e^{\frac{k \cdot T}{\tau}}}{\tau} \cdot dT \cdot \sum_{n=1}^{N-k} n \cdot B(N,n+k) \cdot \left(S \cdot e^{-\frac{T}{\tau}}\right)^{n+k} \cdot U^{N-n-k} \qquad (3.9)$$

where, as defined above, *T* is the ‘‘Time Between Photons”. Although this is a summation over many thousands of terms, we may take $(Se^{-T/\tau})$ to be small and truncate the summation, thereby allowing an efficient computation. For this case, also the variables *S* and *N* always appear together as (*SN*) with excellent approximation provided *N>>(k+n)*.

Figure 11 and Figure 12 show distributions of the time between consecutive detected photons, respectively for *k*=1and 3. Different values of *NS* are considered. As suggested from the behavior shown in these figures, one can demonstrate that, when *NS*<<1, the TBP follows a simple exponential decay curve with a slope of $-1/\tau$. This result at first seems to make little sense because *NS*<<1 implies that the number of photons detected for each projectile is much less than ONE,

and yet the TBP theory applies to the measurement of the time difference between TWO consecutive detected photons. This is not really a problem however, because while *NS*<<1 there still is a small probability of producing two or even more photons. This is also a very important result because it indicates that the analysis of TBP data is considerably simplified by reducing *N* (e.g. by using very thin films) or *S* (e.g. by using filters or high thresholds on the timing electronics) so that *NS*<<1. When this case is satisfied the logarithmic slope of the TBP curve provides $1/\tau$.

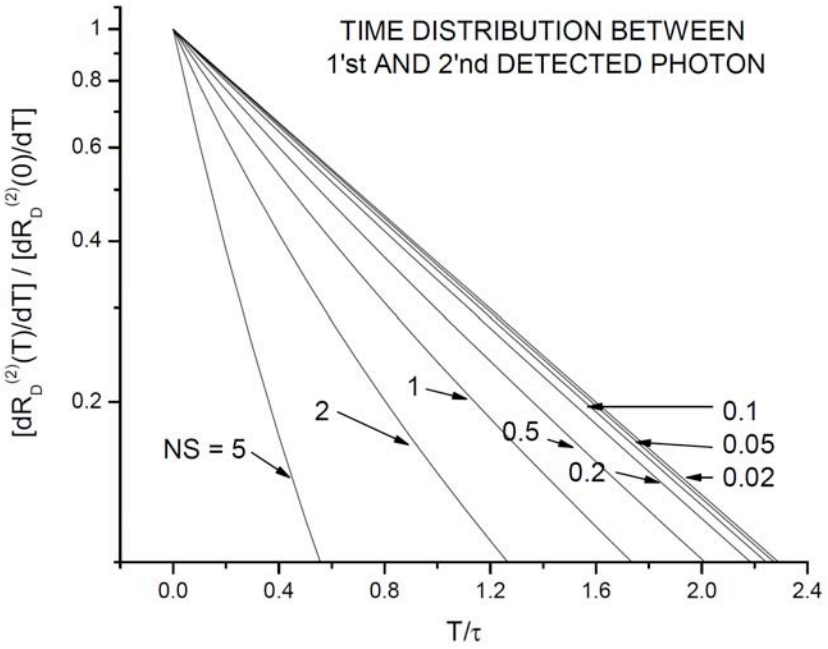

Figure 11 Theoretical distribution of elapsed time between1st and 2nd detected photons

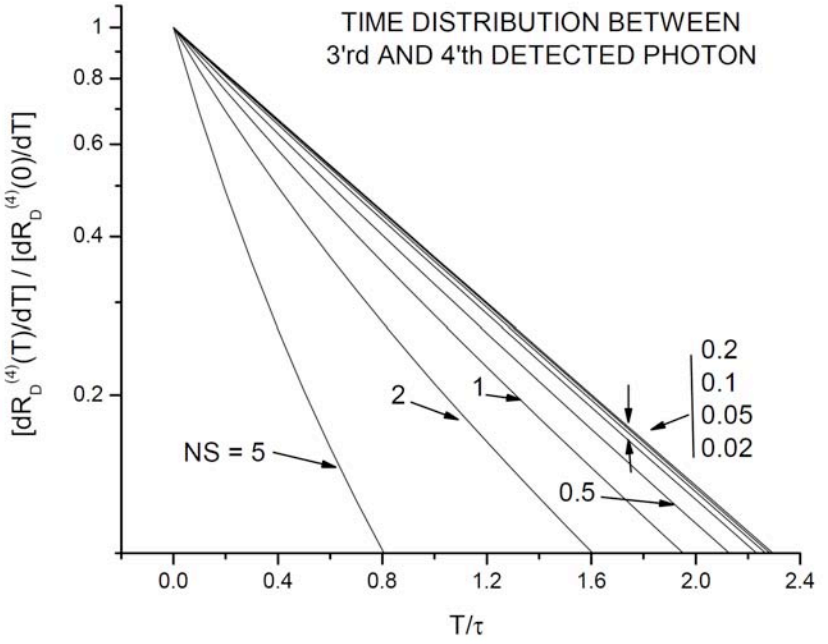

Figure 12 Theoretical distribution of elapsed time between 3rd and 4th detected photons

4. SEARCHING FOR THE IDEAL LUMINESCENT FILM

4.1. Basics of Ion Luminescence

In order to tailor the materials properties of the luminescent film to suit the needs of the IPEM system, a physical understanding of IL is needed. More specifically, a fundamental understanding is needed of the interactions between the bombarding ions and the luminescent coatings and how these interactions govern the properties of the light emitted. This section will progress from the basic physics occurring during ion irradiation through the application and possibilities of various films for the IPEM application.

4.1.1. Electromagnetic Interaction of Radiation in Matter

Fundamental particle physics states that any type of moving charged particle will lose energy as it passes through and interacts with any other medium. The energy loss of non-relativistic particles will mainly be a result of the electromagnetic interactions, which consist of exciting and ionizing atoms close to the ion trajectory, as it passes through the medium (the collision processes). The ionization referred to is globally defined, as the formation of electron-hole pairs, which is essential for both the generation of light and charge in the IL material and the DUT, respectively. Subsequent collision processes mediated by the electromagnetic field associated with charged incoming particles and medium targets (bound electrons and nuclei) lead to the formation of the primary ionization. For heavy particles, the collision energy loss (dE/dx) is also referred to as the stopping power. This energy loss process is a statistical phenomenon, where the collisions responsible for energy losses are a series of independent successive events [15,16].

Another important electromagnetic interaction occurs when atoms or ions having velocities much larger than the electron orbital velocity go through a material. These particles will not only modify the electronic configuration of the media it passes through, but will also modify their own charge state. At sufficiently high energies, their electrons will be stripped and bare nuclei will proceed to lose energy by collision loss processes with the atomic electrons. As this bare particle passes, the probability of electron capture will increase as the particle velocity approaches values close to that of the orbital electrons. The combined probabilistic changes in both the bombarding ion and the medium into which it travels results in a myriad of factors that can potentially play a role in when and how much energy from the incident particles will be deposited into the target material [15,16].

4.1.2. Ion Beam Induced Luminescence – Introduction

Ion Beam Induced Luminescence (IBIL) is a useful materials characterization method, which provides information about the chemical makeup and bonding structure in materials, as well as about ion beam modification on the luminescence properties of solids. Also, the large penetration depth of MeV ions offers several advantages over the relatively shallow penetration of keV electrons typically used in cathodoluminescence. The fundamentals of this technique will provide the basis for the materials design and selection of the IL films used in the IPEM system. Ion luminscence is caused by energetic ions penetrating matter, which cause the formation of electron-hole pairs, as discussed above, that then result in electron transitions and recombination

processes within the outer electron shells of the sample atoms that are prone to luminescence. Luminescence is the nonthermal emission of light by matter, which was excited by an energy absorption process. Luminescence differs from other types of light emission (e.g. reflected and refracted light, Rayleigh scattering, Raman scattering, Cherenkov and laser radiation) by the fact that there are intermediate processes between the absorption and emission of the light. These intermediate processes disturb the correlation between the characteristics of absorbed and emitted photons, such that the resulting spectrum is determined by properties of the substance. Luminescence processes occur in gasses, liquids, and both organic and inorganic solids. In organic solid materials, molecular excitation causes luminescence with transitions typically involving the vibrational modes of the solid. Luminescence from inorganic solids is usually associated with impurities, excited states of isolated atoms, ions, or defects. Luminescence has to constantly compete with nonradiative (NR) processes, with such mechanisms stemming from surfaces and interfaces, deep-level impurities and complexes, spatially extended crystal defects (dislocations), and Auger-related processes. The major characteristics of luminescence in any material include power, spectrum, polarization, energy and quantum efficiency, rise and decay time, excitation spectrum, and light sum [15,17,18].

To better understand ionoluminscence, first it is best to consider and then compare the related topic of photoluminescence, a well-known and understood technique. With photon excitation, light is absorbed with an exponential profile as it penetrates the material. This exponent is determined by the absorption coefficient. Since the absorption coefficient varies over many orders of magnitude from below to above the band gap, the penetration depth can be varied from 10s of nanometers to centimeters. Photo-excited carriers will thermalize and diffuse into the material, with the bulk diffusion length depending on the carrier recombination time, temperature, mobility, and presence of internal fields. Photoexcitation can occur with continuous wave, pulsed, or ultrafast light pulses.

In comparison, the fundamental mechanism for IBIL is initiated when a MeV ion creates electron-hole (e-h) pairs in a solid. A radiative recombination of this e-h pair then gives rise to luminescence phenomena. Several radiative recombination mechanisms are possible, and are generally dependent on sample temperature, valence state of any impurity atoms, and the defect concentration. For this reason, quantitative luminescence measurements are often difficult. Since the intensity of the light output is directly proportional to the generation rate of electron-hole pairs, it can be advantageous to use an ion beam as an excitation source, especially for materials where the probability of radiative recombination is low. For example, Figure 13 demonstrates how a 20 keV electron will deposit almost all of its energy in the top few microns of material, while a 3 MeV proton will penetrate much farther, allowing one to probe deeply buried structures [15,17,18].

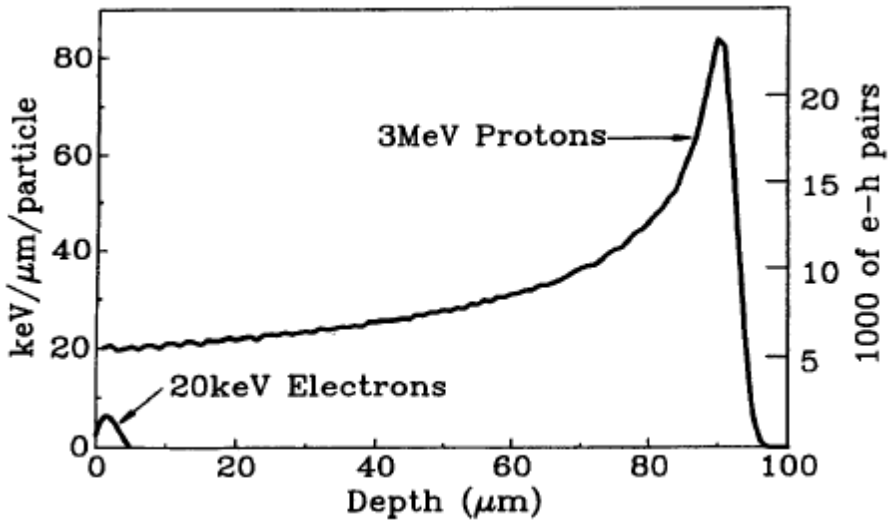

Figure 13 Production of e-h pairs versus depth for cathodeluminescence (20 keV electrons) and IBIL (3 MeV protons) [17]

Ion bombardment of solid surfaces gives rise to a number of elastic and inelastic collision processes. Elastic energy losses experienced by the incident projectile result in the displacement of target atoms and the formation of a collision cascade. On the other hand, inelastic collisions also require active participation from electrons and are the source of a wide variety of additional phenomena (such as emission of secondary electrons and ions as well as electromagnetic radiation). Optical emissions generated by the impact of heavy particles on surfaces are due to excited sputtered target atoms, ions, and molecules, and to backscattered projectiles, which subsequently decay by light emission in the visible and ultraviolet range. Collisional excitation of molecules on the surface of the solid and radiative recombination of electron-hole pairs inside the solid may also contribute to photon emission [15,16].

In summary, the interactions between the ions penetrating the sample and the sample atoms lead to energy deposition within the material. The generation of luminescence can be described by the following processes [18]:

1) Ionization of sample atoms due to the energy deposition in the sample
2) Recombination of electrons and ionized atoms
    a. The lattice absorbs the released ionization energy
    b. Excitation of the "optical system"
3) De-excitation due to radiationless recombinations of excited states
4) Luminescence due to recombinations of excited states

4.1.3. IBIL in Semiconductors

With particle beam excitation, semiconductor atoms are ionized, the lattice will absorb some of the energy, and the electronic states are excited causing both radiative and nonradiative recombination. The electronic structure of crystalline solids can be described by energy bands, which provide delocalized excited states for electrons. Defect centers can locally modify the electronic structure of the solid, causing localized excited states (energy levels in the band gap of semicon-

ductors). Intrinsic luminescence therefore occurs from free electrons in the conduction band combining with holes in the valence band and excitons. It also includes the recombination of excitons bound to defect centers, electron transition from excited states of a defect center to its ground state, and the transition of a charge carrier from a delocalized state.

Many materials contain impurities, which may contribute to luminescence. Extrinsic luminescence may be seen from these impurities, which can act as activators, co-activators, and quenchers. Figure 14 demonstrates this behavior. The shape and the full width at half maximum (FWHM) of the luminescence spectrum will depend on thermal effects and the strength of the interaction between the electrons and phonons, which participate in the optical transition. Assuming low temperatures and weak electron-phonon interactions, the luminescence spectra will consist of sharp peaks and narrow bands. Strong electron-phonon interactions will result in a broadening of the peaks and bands in the spectra.

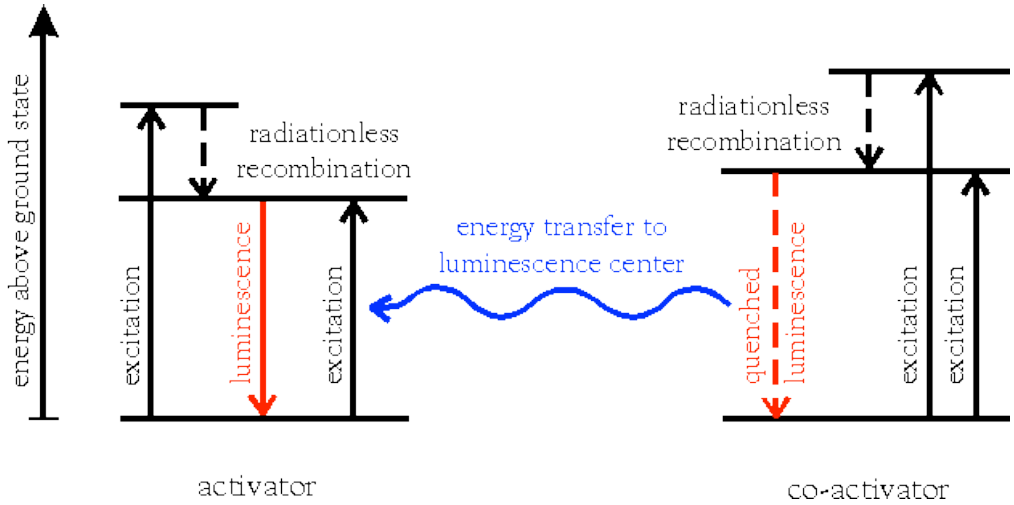

Figure 14 Energy transfer process between co-activator and activator [18]

4.1.4. Selection of Materials

Since the IBIL characteristics of the IPEM film will be utilized, studying various materials for their IBIL spectra and lifetimes was critical to the progress on this project. There are a variety of considerations and requirements that need to be met for the ideal material. These considerations include:

- Ion beam excitation volume – this volume will be dependent on the ion beam's energy and the stopping power of the material. Since the penetration will be significant, the excitations will include both volume and surface excitations.

- Detectability – the emitted wavelength of light should correspond to high spectral sensitivity of the detector. The response of most detectors is more sensitive to visible light than ultraviolet light.

- Quantum efficiency of luminescence – The luminescence efficiency should be high for maximum sensitivity. Non-radiative recombination processes should be mini-

mized, including non-radiative point defect, dislocations, inclusions, grain boundaries, and surfaces.

- Time response – The time response of the luminescence should be fast so that time resolution can be high and accidental coincidences can be limited. Therefore the recombination mechanism should be characteristic of the fastest recombination mechanism possible considering the spatial and spectral characteristics of the excitations in the probed volume.

- Handling – The film should be easy and fairly inexpensive to produce, as well as easy to handle and apply to samples/devices.

- Radiation Damage Tolerance – The material should be able to withstand radiation bombardment both in air and in a vacuum with no adverse effects on the luminescence properties.

- Homogeneous Luminescence – The luminescence properties should be homogeneous across the entire film such that any ion strike point results in a similar response.

Common materials used as scintillators for radiation detection provided initial candidates to consider and include inorganic crystals, organic plastics and liquids. Liquids are not feasible for this application, as the sample must be mounted perpendicular to the ion beam. Plastic scintillators are reliable in their field, but experience aging and lose light yield with time, solvents, high temperatures, radiation, or mechanical loading. In addition, their surfaces can be damaged by the formation of microcracks, atmospheric quenching, and radiation, leading to the formation of color centers. Considering this, a combination of material types were investigated for their IBIL properties. These included Bicron BC400, which is a commonly-used plastic scintillator supplied by Saint-Gobain; P47, a ceramic powder with the composition Y_2SiO_4:Ce; and gallium nitride (GaN), a III-V semiconductor being extensively studied for its application in solid state lighting. The stability and tenability of GaN-based scintillators resulted in an extensive study into their ionoluminescence properties.

4.2. GaN and InGaN/GaN Quantum Well Structures

4.2.1. Potential of GaN and InGaN/GaN QWs

One material whose light properties have come to the forefront of materials research over the last decade is gallium nitride (GaN). In addition to its potential application in solid-state lighting, it is an interesting material as a scintillator for detecting ion bombardment. In general, good scintillators are characterized by high light output and short luminescence decay times. The shorter the duration of its luminescence, the less “dead time,” and the more ionizing events per unit time it will be able to detect. In contrast to plastic scintillators, GaN is not subject to the aforementioned degradation mechanisms. A series of GaN samples with various doping levels were investigated, and their properties will be discussed. After these initial studies, it was recognized that bandgap engineering could be used to create an “ideal” structure.

Bandgap engineering works by designing the semiconductor epitaxial structure to meet the necessary requirements for the desired optical response. Tailorable parameters include layer thickness, layer alloy composition, spatial positioning of layers, choice of substrates, choice of unintentionally doped or doped materials, and growth rates. One major limitation to the use of tailored GaN is the time and cost-intensive process required to produce GaN structures.

4.2.2. Design of InGaN/GaN QW Structure

The structure illustrated in Figure 15 was chosen based on the listed requirements and the growth time restraints. The overall structure had to be relatively tall to collect a significant fraction of the ion-beam excitation volume, so a thickness of five micrometers was chosen. To minimize the effects of surface recombination and maintain high ionoluminescence quantum efficiency, wide bandgap AlGaN barrier layers were included both at the substrate interface and at the terminal interface of the semiconductor structure. A sapphire substrate was used and three microns of an undoped buffer layer was grown to limit the strain induced by lattice mismatch. Within the active region of the structure are InGaN quantum wells, which produce blue luminescence with high efficiency.

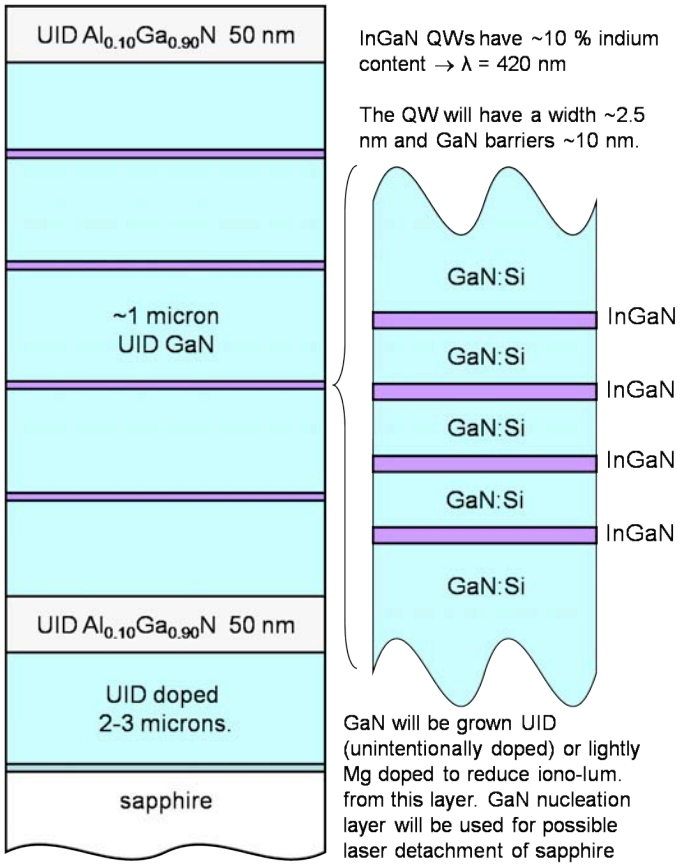

Figure 15 Schematics of the InGaN/GaN quantum well engineered for ionluminescence

Figure 16 shows an energy band schematic of the semiconductor structure, as well as the spatial distribution and dynamics of the electron-hole pairs generated by the ion beam. For ion beams with penetration depths of approximately 50 micrometers, the semiconductor represents only a

small portion of the total activated volume. However, the photons produced per unit length of semiconductor material are quite high. The buffer layer is undoped and relatively low in efficiency, comprising many defect states and nonradiative recombination (NR) centers. Unintentional doping (UID) and residual deep states contribute to a small amount of yellow luminescence. There is also residual ultraviolet (UV) luminescence from unthermalized carriers in the active region. The amount of UV to blue luminescence is influenced by the carrier diffusion length relative to the spacing between the multiple quantum wells.

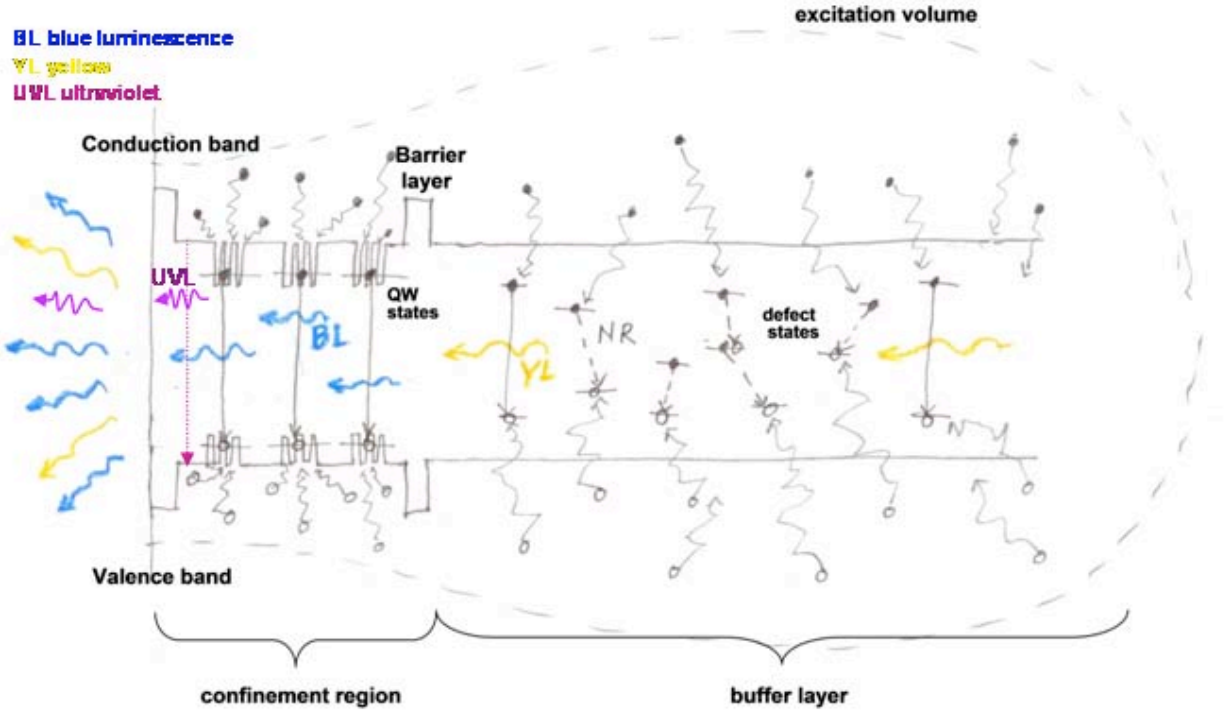

Figure 16 Energy band schematics of a quantum well heterostructure designed for operation as and efficient blue-emitting scintillating material for detection of ion beam irradiance

In the active region of the semiconductor, there are quantum wells formed with very thin InGaN layers that effectively collect carriers as they thermalize to lower energy states after generation by ionization. Also, the AlGaN barrier layers surrounding the active region protect the carriers from surface and interface states that harbor high densities of nonradiative recombination centers. As a result, most of the carriers generated in the active region are funneled to the quantum well states where electrons and holes recombine with high efficiency. The efficiency of recombination is much higher in a quantum well than bulk GaN because of the high degree of spatial localization of the electron and hole wavefunctions with the confining well. The quantum wells emit blue light that is transparent to the surrounding GaN material. Thus the blue light is effectively coupled out of the semiconductor structure for external detection. Along with the blue light, there is a small amount of yellow luminescence from the buffer layer and GaN barrier layers. Figure 17 demonstrates an experimental PL spectrum of this grown structure, which shows high blue and lower yellow luminescence efficiency.

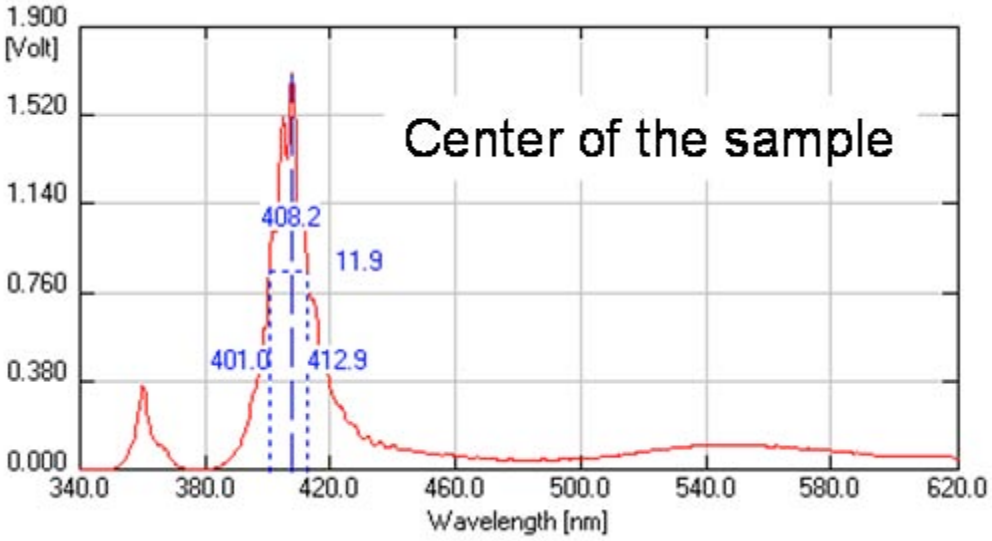

Figure 17 Photoluminescence spectrum of InGaN/GaN quantum well structure shown in previous figure

4.2.3. IBIL of Quantum Well Structures

Another experiment of IBIL on these quantum well structures was carried out using two different energies of a proton beam. One major advantage of IBIL is the ability to vary the energy of the ion beam to significantly change the penetration depth, and thus the depth into the structure from which one can obtain information. With 50 keV protons penetrating approximately 300 nm in GaN, and 250 keV protons penetrating approximately 1400 nm in GaN, Figure 18 depicts the depth into the "old" and "new" InGaN/GaN quantum well structures these beams probe. Figure 19 shows the IBIL spectra for these two quantum well (QW) structures, as well as n-type GaN and bulk InGaN samples. The 50 keV protons are seeing all of the QWs in the old structure, and a few hundred nanometers into the InGaN underlayer; while the 250 keV protons are penetrating through the QWs (without depositing an extensive amount of energy) and a significant amount into the InGaN underlayer. Therefore, the 50 keV protons are depositing more of their energy in the quantum wells, and a larger blue bandedge emission band is observed. The 250 keV protons result in much more intense yellow band light, which is explained by them penetrating into the InGaN underlayer. In this case, the yellow light is coming from defects in the GaN lattice.

For the new structure, the 50 keV protons are stopped and deposit all of their energy in the QWs, while the 250 keV protons penetrate through the QWs and into the InGaN underlayer. Even with the 50 keV beam, yellow light is observed, suggesting similar defect light is created in the InGaN/GaN QW structure. Again, the intensity of the yellow band increases significantly with the 250 keV beam, as it penetrates into the underlayer.

Through the use of band gap engineering the light quality of light produced by the GaN and InGaN films were altered significantly. Despite this, several other scintillating materials were investigated by a variety of techniques described in the next subsection.

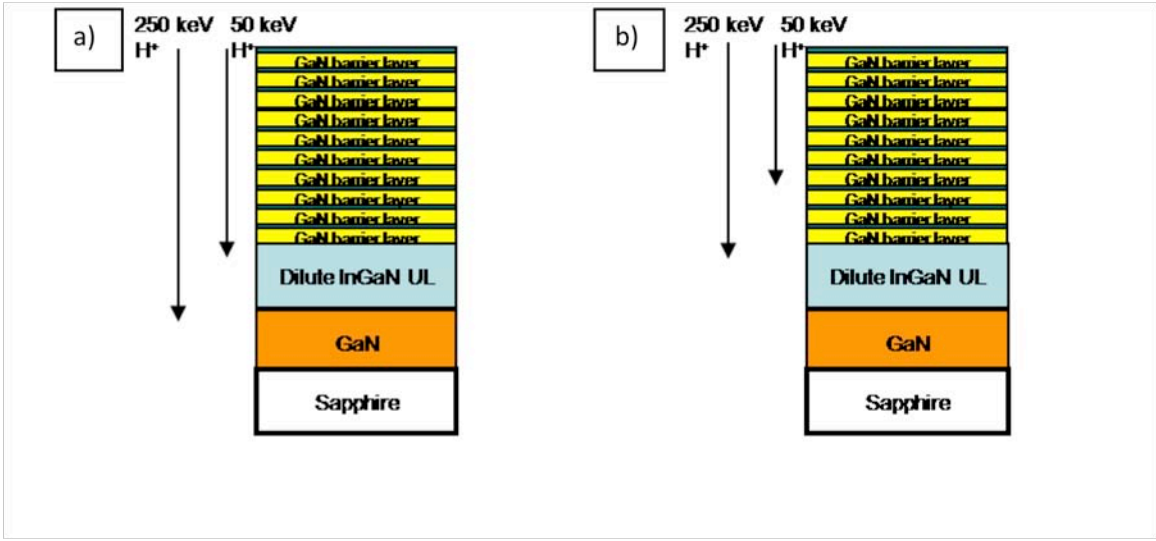

Figure 18 50 and 250 keV H^+ beam penetration in a) old quantum well structure with ~63 nm of quantum wells, and b) new quantum well structure with 430 nm of quantum wells. Note these structures are different from that described in Figure 15

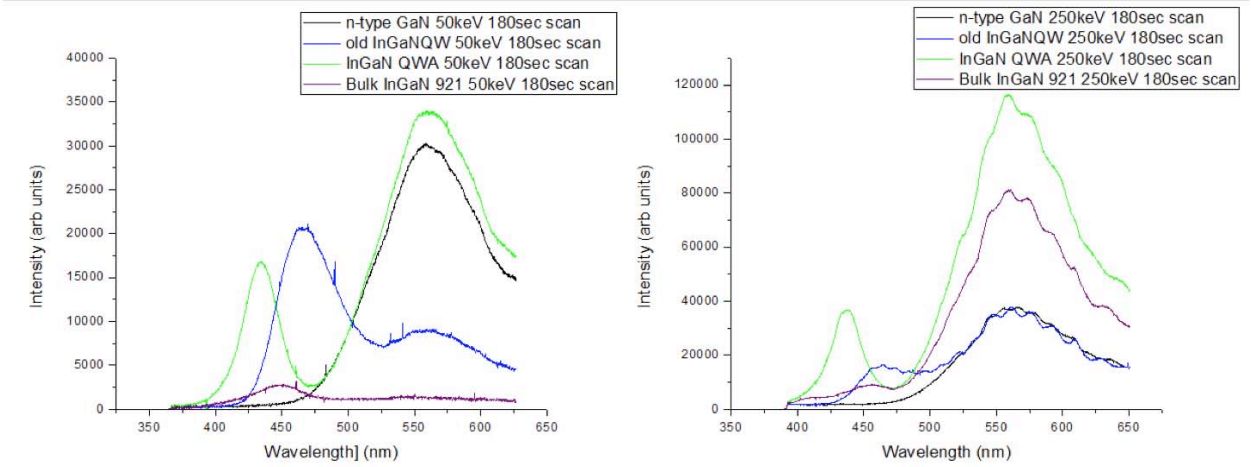

Figure 19 IBIL spectra of various samples using a 50 keV and 250 keV proton beam in attempt to probe different depths in these structures

4.3. Comparison of the Various Luminescent Materials

4.3.1. Experimental Methods

a) Photoluminescence

Photolumininescence (PL) experiments on the materials of interest were carried out using a handheld UV lamp as the excitation source and an Avantes fiberoptic spectrometer to collect the light. The spectrometer has a sensitivity region covering 200-1100 nm. PL is a quick and easy method to obtain a general idea of the optical properties of each sample produced.

b) IBIL

IBIL experiments were carried out using a handheld Po-210 alpha particle source, an implanter, and a van de Graaff tandem ion accelerator. Thus, the excitation sources included 2.7 MeV alpha particles, 50 and 250 keV H^+ ions, and 7.5 MeV He^{2+} ions. Spectrometers were used to collect the light emitted as intensity versus wavelength.

c) IBIL Lifetimes

As discussed previously, luminescence processes are characterized by intermediate processes between the absorption and emission of light, and these processes will have a characteristic lifetime that offers information about the material and band structure. For the IPEM application, the lifetime of the luminescence is a critical parameter. Since electronic and optical signals are being put into coincidence to form an image with the best-achievable resolution, the timing must be well matched. For example, as each ion strikes the luminescent film, it will produce light for a given amount of time. If another ion strike occurs before the luminescence from the first strike completely decays, it is possible that an accidental coincidence will occur. This can severely degrade the resolution system, since the wrong *x* and *y* coordinate will be recorded for that ion. When performing lifetime experiments, ion excitation was used as in IBIL, and a photomultipler tube (PMT) was used to measure the light output in terms of voltage. In this approach, the voltage induced on the PMT was measured, and the 1/e decay time was calculated. In addition, a time between photons (TBP) method, as developed by Brice [14], was used in conjunction with a single photon position sensitive detector. A combination of experimental results and theory was used to determine the lifetimes of the materials with this approach.

4.3.2. Results

a) Photoluminescence

An example of a PL spectrum can be seen in Figure 20, which clearly shows the effect of introducing quantum wells in to the structure, as well as the effect of the amount of indium, which shifts the bandgap to longer wavelengths. While PL induces different optical processes than IBIL, it does provide an initial estimate of the expected wavelengths, allowing for a rapid narrowing of the potential materials.

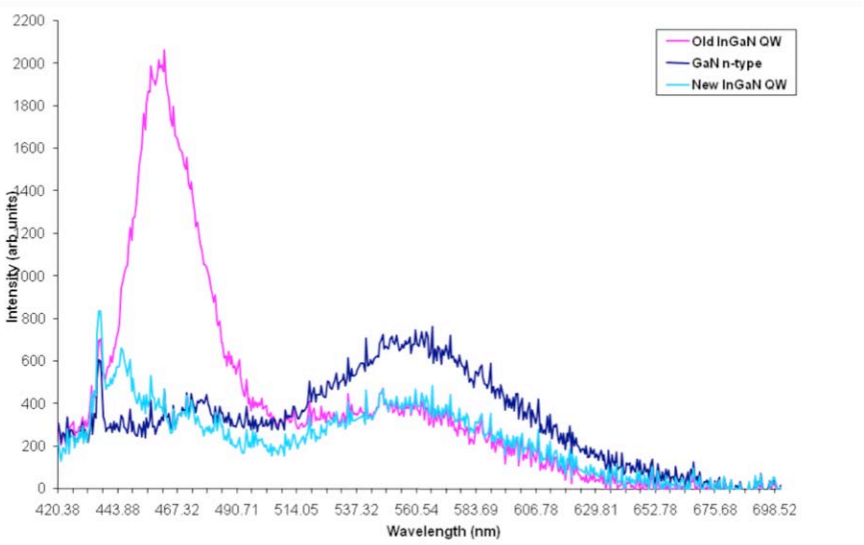

Figure 20 PL spectra of n-type GaN and two InGaN/GaN quantum well structures

b) IBIL

Figure 21 is a series of IBIL spectra collected on the implanter using 250 keV H^+ ions. As seen in the plot, the P47 produces significantly more light than the other materials (it is on a separate y-scale of arbitrary, but consistent units), with the InGaN/GaN quantum wells the next brightest. In Figure 22, the response of the bialkali photocathode used on the detector is included. Considering how the sensitivity can drop off rapidly, matching the material emission to the photocathode response is critical. This plot clearly demonstrates that the bandedge emission for InGaN/GaN quantum wells, as well as the emission wavelength of P47 nicely matches the detector efficiency; while the yellow defect band from GaN is not at the ideal wavelength, and occurs where the spectral efficiency drops off dramatically.

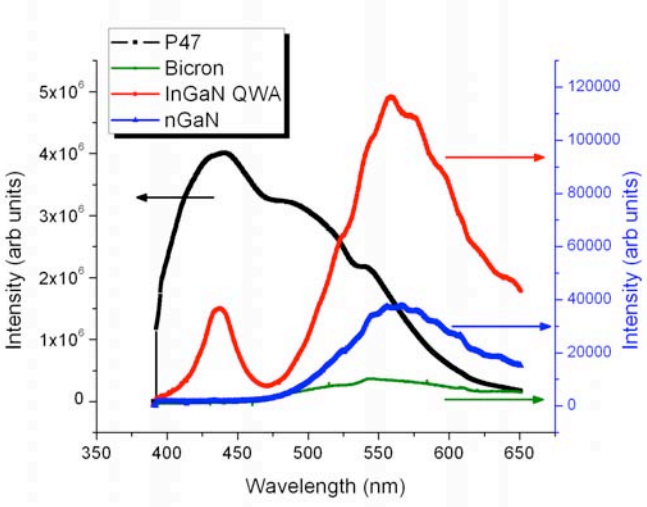

Figure 21 IBIL spectra taken with 250 keV H^+ ions of the various materials studies for the IPEM film

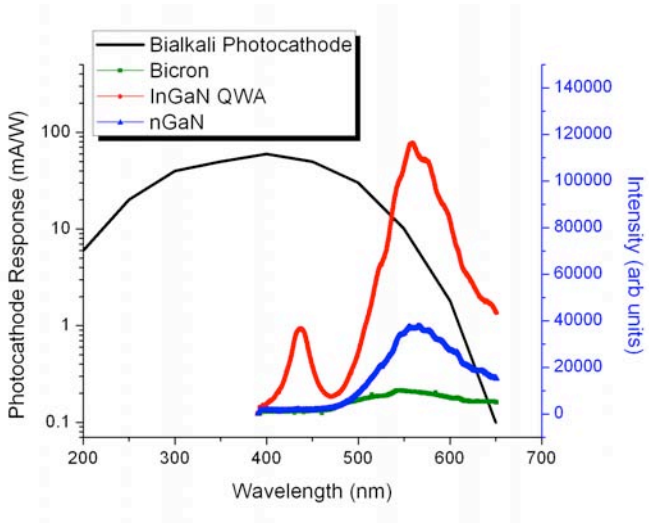

Figure 22 IBIL spectra plus bialkali photocathode response curve. Note that the photocathode response is plotted on a log scale

After the initial experiments of IBIL intensity demonstrating the emission spectrum will work based on the detector utilized, photons per ion measurements were carried out in an attempt to maximize efficiency. While IBIL gives relative intensities, an actual measurement of photons detected per ion with the same setup and optics to be used in the IPEM application is useful. Therefore, 7.5 MeV He^{2+} ions were brought incident onto the materials. A PIN diode was used to count the number of ion strikes, and the light emitted was collected with a microscope and each detected photon seen by the position-sensitive detector was counted. Figure 23 represents the results from this experiment. It is clear based on this work that the InGaN/GaN quantum wells are the most efficient light emitters when dealing with the IPEM system limitations.

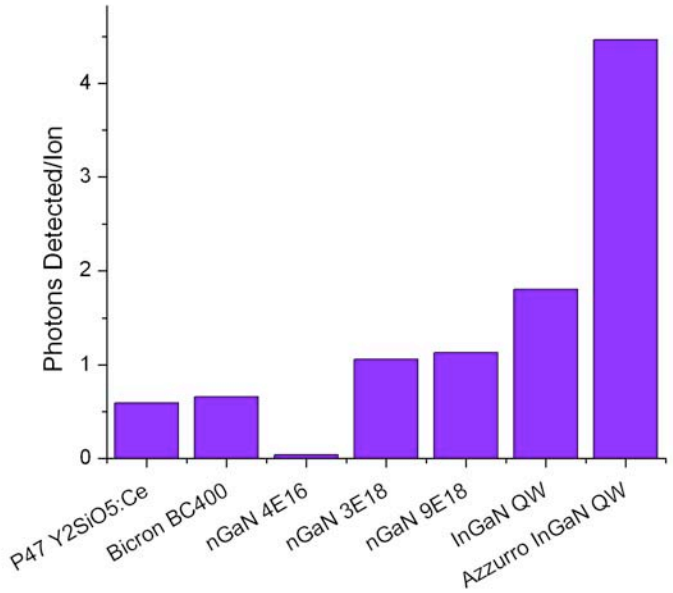

Figure 23 Photons detected per ion as measured with a 7.5 MeV He^{2+} beam. InGaN/GaN quantum wells are clearly the brightest

c) IBIL Lifetimes

Figure 24 portrays typical results from a lifetime experiment on InGaN/GaN QW samples. The IBIL spectrum shows two characteristic emissions. The shorter wavelength emission is the bandedge emission, which is typically very fast. The broad longer wavelength band is indicative of defects in the GaN structure. Since the defect structure will allow for various paths of recombination and energy release, including traps and non-radiative processes, the lifetime of this light tends to be much longer. In the experiment, filters were used to look at just the bandedge, and just the defect emission light. In Figure 24, the very different lifetimes obtained for these two experiments are displayed. The bandedge emission has a very short lifetime, which was faster than the resolution of the oscilloscope being used (nanoseconds), while the defect emission was measured to have a lifetime on the order of hundreds of microseconds. Figure 25 shows these two lifetime measurements more clearly.

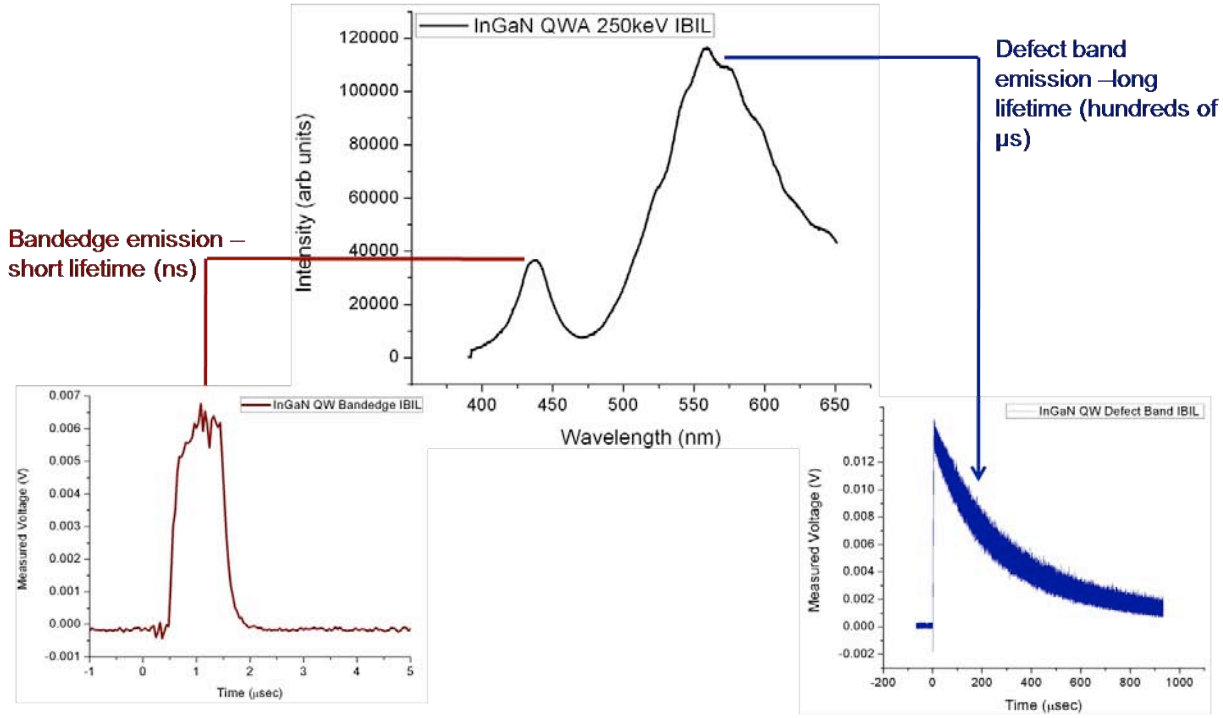

Figure 24 IBIL spectrum and corresponding lifetime measurements for the two major emission bands

As mentioned previously, lifetimes were also calculated using the Brice time between photons (TBP) theory. In these experiments, the samples used were free-standing films mounted on top of a PIN diode. The diode was used to count the ion strikes, since the photons/ion is a necessary parameter for fitting the data. The light emitted was collected with a single photon position sensitive detector. These experiments were carried out without filters such that the lifetime measured is representative of the material as a whole and does not distinguish between bandedge and defect band light. Figure 26 displays TBP data measured and calculated for an n-type GaN sample doped with 1E17 cm^{-3}, and an InGaN/GaN quantum well structure fabricated by Azzurro Semiconductor, respectively. The resulting luminescence lifetime for the n-GaN was 1300 µsec, and that for the QWs was 460 µsec. Therefore, the QWs also have an advantage in terms of lifetime, with a lower possibility of accidental coincidences.

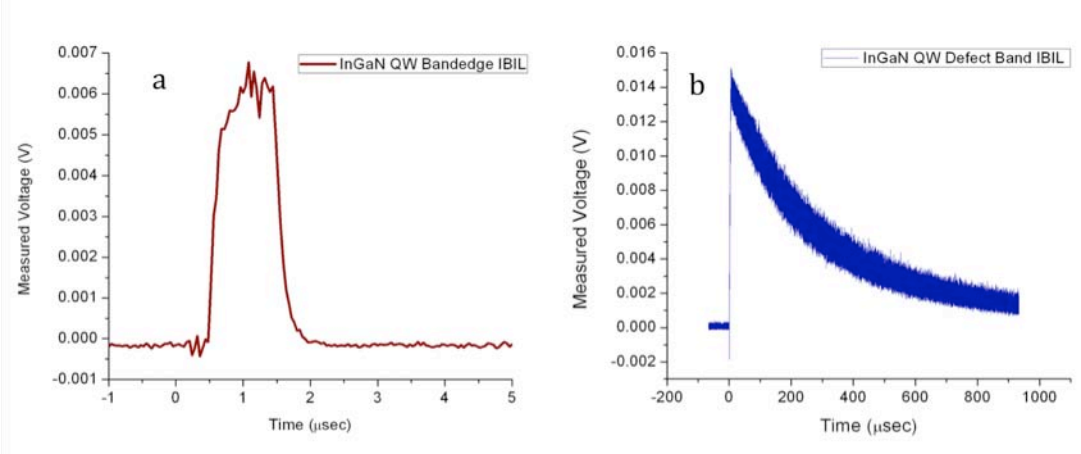

Figure 25 Luminescence lifetimes of a) bandedge and b) defect band in InGaN/GaN quantum wells

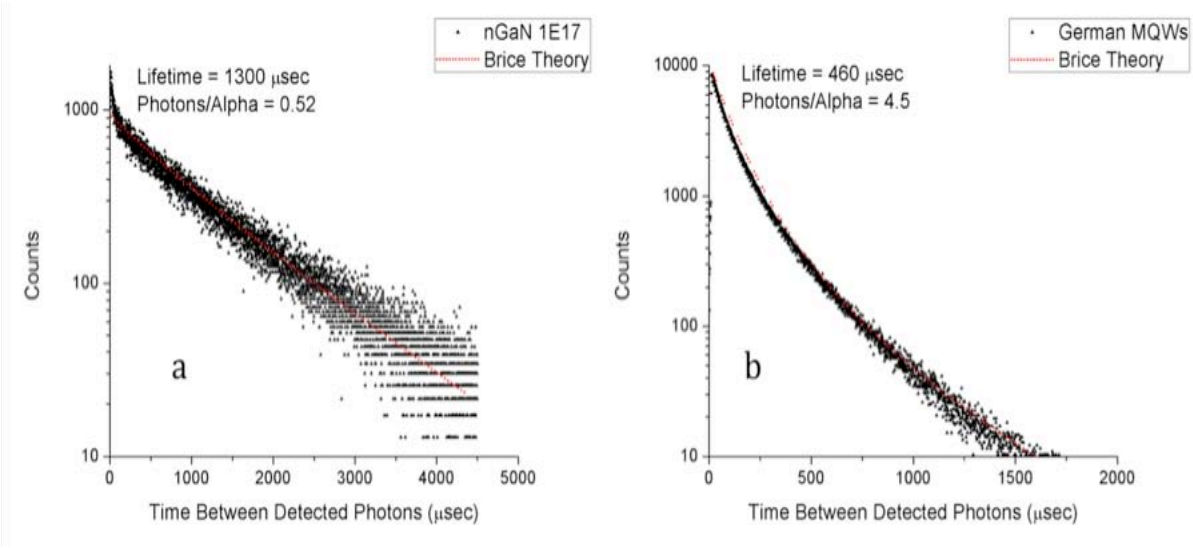

Figure 26 TBP luminescence lifetime for a) 1E17 cm^{-3} n-type GaN and b) InGaN/GaN quantum wells.

5. IPEM INSTALLATIONS

5.1. IPEM at the SNL IBL's tandem accelerator

In preparation for installing an IPEM system on one of the United States' high-energy cyclotrons, we designed, built, and installed a similar setup on Sandia's tandem accelerator and began initial experiments. Using a beamline with a nuclear microprobe, we have been able to compare results obtained with a scanning focused beam to those from the IPEM. A JEOL OM-40 microscope with 20x magnification and a 0.3 numerical aperture is used, in conjunction with a series of lenses and a PSD. A photograph and a schematic of this setup are shown in Figure 27.

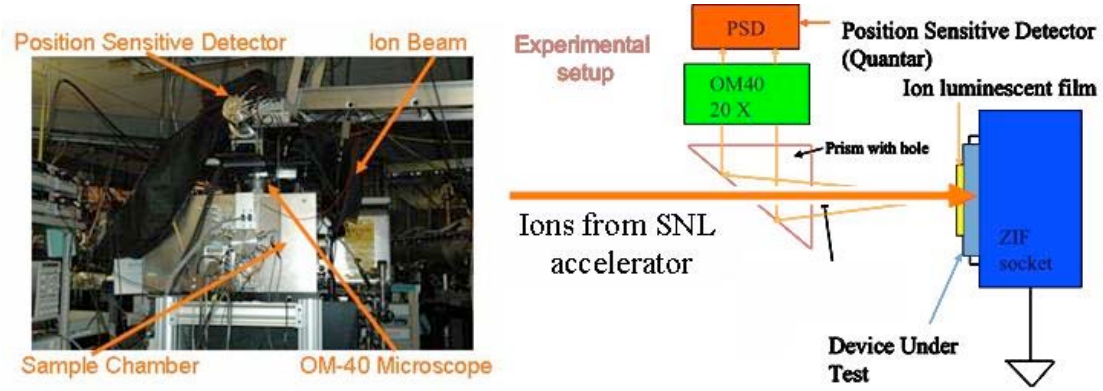

Figure 27 Photograph and schematic setup of the IPEM on the SNL tandem accelerator

The overall efficiency of the optical system, taking into account transmission through the microscope and the solid angle is 0.001 (we will detect 1 photon for every 1000 generated). Based on the experience of setting up this system, we have encountered a variety of obstacles. We need to design the optics to obtain the desired magnification such that we fill the whole active area (1" diameter) of the PSD, requiring ~60x magnification. The optics, as well as the hardware, need to be configured so an acceptable focus is simultaneously achieved on both the CCD and the PSD. Also, considering the sensitivity of the PSD, the background lights must be minimized so that the external background counts are less than those from the ion beam, reducing the chance of accidental coincidences.

Figure 28 shows simultaneously accumulated IBIC and IPEM-IBIC images of a GaN and TEM grid covered PIN diode imaged with 7.5 MeV He^{2+} ions using the tandem IPEM system. For these experiments, five signals were recorded: the IBIC signal, the *x*- and *y*-position as determined from the microprobe beam scanner (a), and the *x*- and *y*-positions determined from the PSD (b). The scanned IBIC image was created by showing the corresponding IBIC signal for each *x*- and *y*-position, whereas the IPEM-IBIC image resulted from putting the photon signal (and resulting *x* and *y* from the PSD) detected in coincidence with an IBIC signal from the diode. The image shows a 1000 mesh TEM grid, where the sample configuration consists of a diode + grid + GaN phosphor, such that the image of the grid in the right image is strictly an effect of the IPEM technique. The resolution of the scanned image is about 0.5 µm while the resolution of the IPEM image is around 2.5 µm. An IBIC experiment performed on a TA788 SNL made SRAM. Figure 29 shows the IBIC median maps for the scanned microbeam (a and c) and for the IPEM system (b and d). Although, the IPEM image is fuzzier than the scanned image, the n-wells can

be seen quite well. By changing the contrast even transistors in the p substrate are visible (c and d).

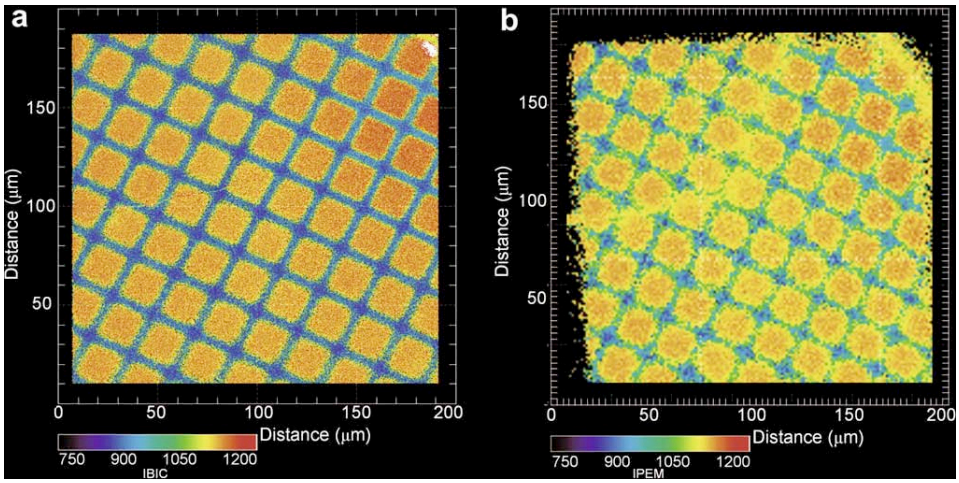

Figure 28 Simultaneous focused microbeam and IPEM images of 1000 mesh TEM grid

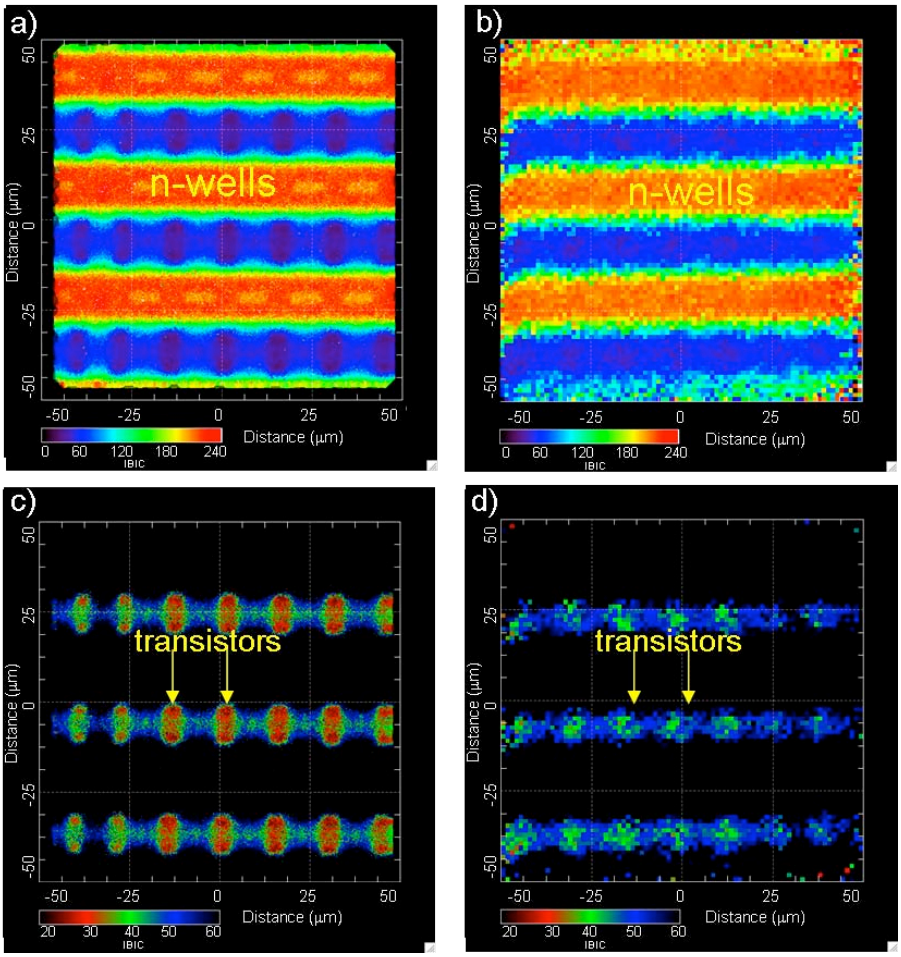

Figure 29 Scanned ion beam and IPEM IBIC images of an SNL TA788 SRM

5.2. IPEM at the LBNL 88” cyclotron

The IPEM has been redesigned for in air operation in the LBNL 88” cyclotron’s Cave 4a. Figure 30 shows the cyclotron facility map indicating the location of the IPEM. The cyclotron ion beam was extracted through a nozzle with a 5 μm Al window. The DUT was placed at 6 mm from this window, which is at the working distance of the OM-40 microscope.

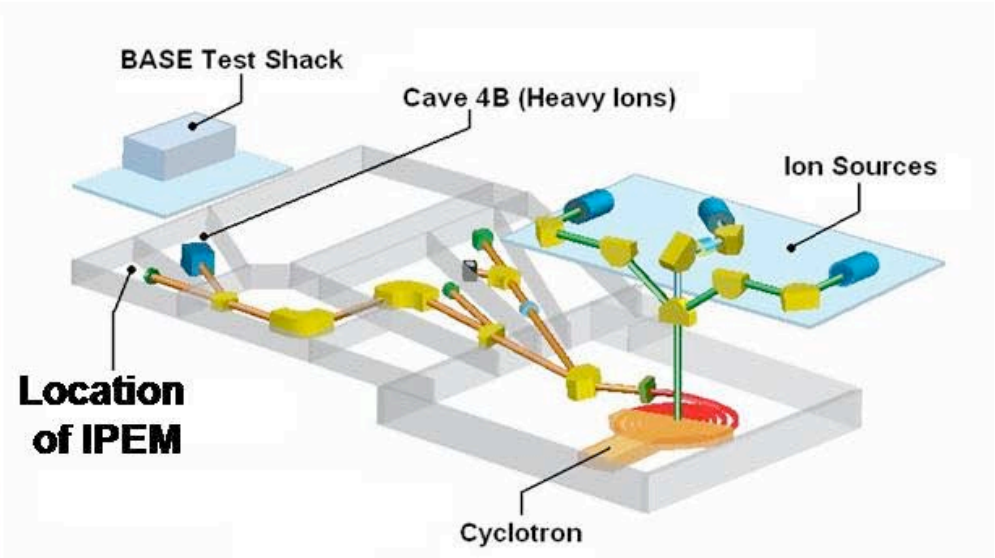

Figure 30 Location of the IPEM at the LBNL 88" cyclotron

This system used a dual microscope setup as shown in Figure 31 where the DUT was viewed through a separate OM-40 connected to a CCD camera. The system was calibrated so that a translation vector took the DUT from the CCD position to the PSD position. The sample stage had three axis navigation and optical or GDS II alignment. Monte-Carlo calculation using the SRIM program showed that the exit foil and the air path would limit resolution to 1 μm. We have performed experiments with several ion beams for the 10 and 16 MeV/amu cocktails that range in energy from a few hundred MeV (light ions) to 1.2 GeV Xe ions.

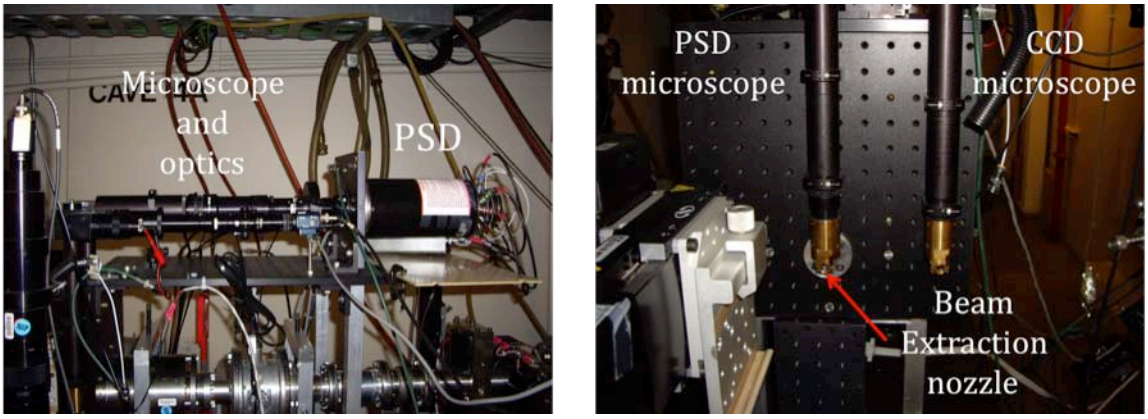

Figure 31 Photographs of the LBNL IPEM setup

We encountered several new difficulties due to the very high energy of these ions, as well as the operation of the IPEM in air. Figure 32 shows an IPEM image recorded at the LBNL cyclotron using 10 MeV/amu Ne ions. The quality of the image is significantly worse that the SNL tandem images. The n-wells can be recognized as the bright bands and we estimate the resolution is > 5 μm.

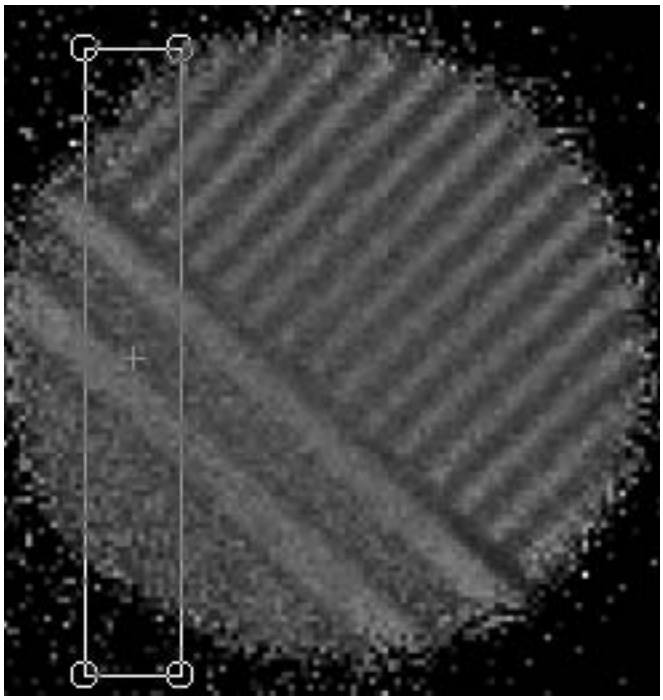

Figure 32 IPEM image of an SNL TA788 SRAM recorded at the LBNL cyclotron's IPEM

We were unsuccessful to get a well-focused image for heavier ions for either our test PIN diode or for the TA788. As it was determined later, the ion luminescence of air (which will be discussed in the next session) was much higher for heavier ions (such as Xe) than for light ions (Ne) making it impossible to get an image in focus at the highest energy range with the current setup.

6. CURRENT STATUS, CHALLENGES, AND FUTURE WORK

After many tests at the LBNL cyclotron with limited success, we suspected that the troubles were caused by luminescence occurring in the air path between the microscope and the device as schematically shown in Figure 33. Please note that the violet light is not real; it just illustrates the air luminescence. Because this light has a shorter lifetime than the GaN IPEM film and is created first, it arrives in the IPEM detector first, and is out of focus. The correlation between the photon's position and the ion strike point is therefore lost, as is the resolution of the IPEM system.

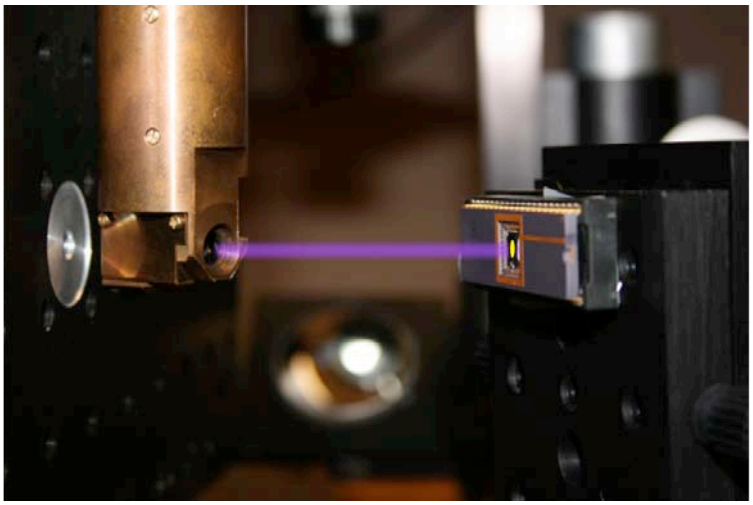

Figure 33 A schematic picture of the air luminescence

To prove this suspicion and quantify the effect, we performed an experiment on the tandem accelerator at SNL. We extracted a 20 MeV C beam into air and measured the photons from the air luminescence using a Hamamatsu R7401 MCP. The number of ions was determined using a PIN diode that the beam was incident on. This way we could estimate the number of photons per MeV created in air. At the same time, the spectrum of the emitted light was determined and found to be in the range of blue-green light.

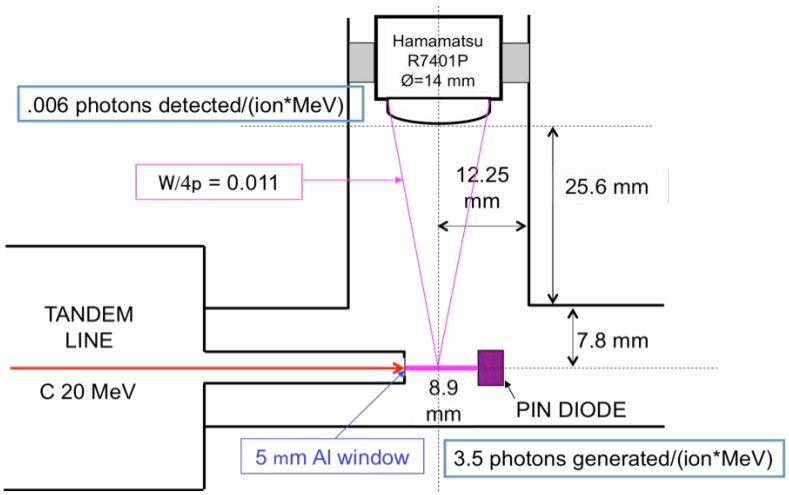

Figure 34 Experimental setup to measure air luminescence at the SNL tandem accelerator

Using the data from this experiment we were able to calculate what ion luminescence intensity we could expect at the LBNL cyclotron for the 10 MeV/amu and 16 MeV/amu beams, as shown in Table 1.

Table 1 Expected ion luminescence intensities at the LBNL cyclotron for the 10 MeV/ amu and 16 MeV/amu cocktails

ION	E	dE/dt	density	dE/dx	Range	path	ΔEinPath	ph/ion
	MeV	MeVcm2/mg	mg/cm3	MeV/cm	cm	cm	MeV	
B	108	1.00	1.25	1.25	50.00	0.60	0.75	**0.02**
O	183	2.53	1.25	3.16	38.50	0.60	1.90	**0.04**
Ne	216	3.70	1.25	4.63	30.00	0.60	2.78	**0.06**
Ar	400	11.10	1.25	13.88	21.10	0.60	8.33	**0.17**
Cu	659	23.90	1.25	29.88	17.60	0.60	17.93	**0.36**
Kr	906	34.50	1.25	43.13	18.20	0.60	25.88	**0.52**
Xe	1232	68.10	1.25	85.13	14.20	0.60	51.08	**1.03**
N	234	1.27	1.25	1.59	83.00	0.60	0.95	**0.02**
Ne	321	2.65	1.25	3.31	57.00	0.60	1.99	**0.04**
Ar	642	8.03	1.25	10.04	41.80	0.60	6.02	**0.12**
Cu	1007	18.50	1.25	23.13	30.80	0.60	13.88	**0.28**
Kr	1226	29.00	1.25	36.25	28.00	0.60	21.75	**0.44**
Xe	1955	56.10	1.25	70.13	23.80	0.60	42.08	**0.85**

Investigating Table 1 carefully it is clear why we were able to get a fuzzy image for 10 MeV/amu Ne beam and nothing at all for the Xe beam. We assume that both beams create at least one detected photon/ion from the GaN film. In case of the Ne beam the air produces only 6 photons for every 100 ions, which appears as a 6% background. On the contrary, the Xe beam produces one photon for every ion and these photons always reach the PSD before the photons from the GaN film over the DUT.

In future design iterations, we plan to make the following changes partially to mitigate the effect of air luminescence and to improve the performance of the IPEM.

- Our two-microscope design proved to be insufficiently precise; we had to recalibrate the system for each position on the DUT that were far from each other. A new system is being designed and tested that uses only one microscope. The light is split into two beams using a partially silvered mirror and the image can be seen simultaneously on a CCD camera (for positioning) and on the PSD (for IPEM measurement).
- To reduce or even eliminate the effect of air luminescent we are planning several things:
    - Since the air luminescence is manly below the wavelength of 400 nm and the GaN spectrum is above that we will employ band filters to reduce the background due to air luminescence.
    - We will use a different photocathode in the PSD, which is more sensitive to longer wavelength. Figure 35 shows the sensitivity of the current photocathode, the future one with the air luminescence and GaN spectra overlayed.
    - New nanophosphors[2] will be used in the future. These will have two advantages
        - The emitted light is in the yellow and red range, which is well separated from the air luminescence spectrum.
        - These new phosphors have a much shorter decay time (ns) than the GaN (100 μs), which will be important for SEU images.

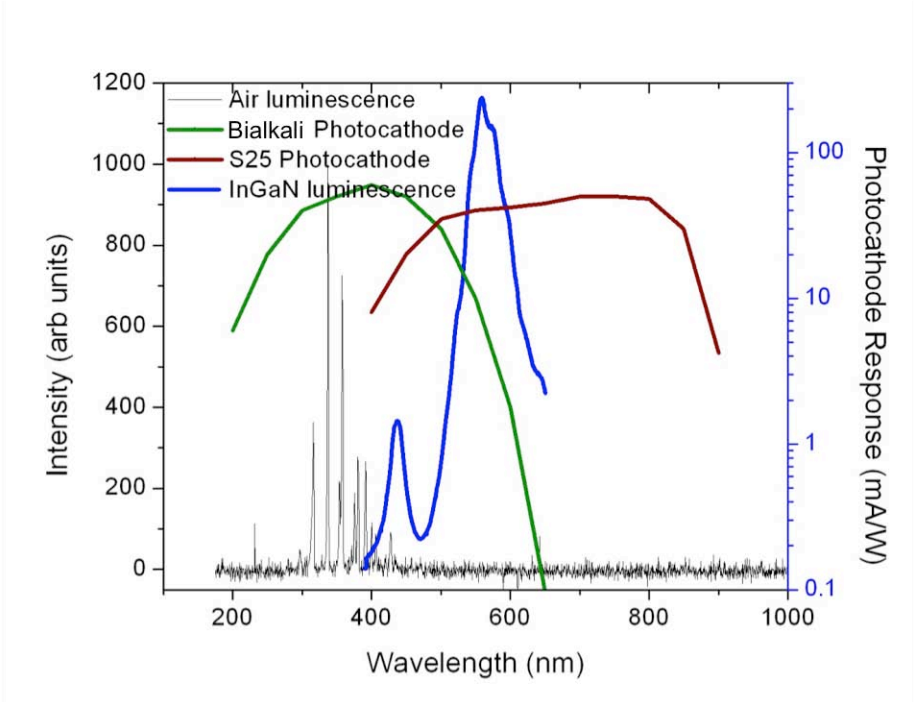

Figure 35 Efficiency curves for the currently used photocathode and of the new PSD with the spectra of air and GaN luminescence

[2] When the project started we were considering these nanophosphors but the light yield was extremely low. During the three years of the project significant progress was made in this field and these nanophosphors look very promising now.

The next version of IPEM will have a dedicated beamlike at the LBNL cyclotron, which will make the long, tedious realignment unnecessary.
Eventually, an IPEM will be installed at the Texas A&M University superconducting cyclotron.

7. CONCLUSIONS

The future of heavy ion radiation effects microscopy depends on the development of scanned microbeams and/or emission microscopes that can be easily used on cyclotrons, which provide GeV-energy heavy ions. This poses some serious design and engineering obstacles, but is critical for the radiation effects community to continue having the ability to study and improve circuits and devices that are immune to Single Event Effects (SEEs). The IPEM technique provides a reasonable solution to the issues, and the continuing progress in its development is promising. A variety of materials have been extensively studied for their IBIL, lifetime, and radiation tolerance characteristics. Significant energy was put into developing the ideal InGaN/GaN quantum well structure, using bandgap engineering to optimize the fast bandedge emission. Results demonstrating good comparison between traditional nuclear microscopy and IPEM imaging have been seen on SNL's tandem accelerator and presented. The newest IPEM system has been designed, developed, and installed on LBNL's 88" cyclotron. Initial results from the cyclotron IPEM have demonstrated its ability to be used as a radiation effects microscope with GeV-energy ions. Work is in progress to develop an improved version of this system, to enhance the optics, fully understand the timing, and optimize the luminescent material. Having the ability to use GeV-energy ions while achieving the desired resolution will allow for the continued use of REM into the future as feature sizes shrink, and the thicknesses of overlayers continue to increase.

8. REFERENCES

1. Dodd, P.E., *Device simulation of charge collection and single-event upset.* IEEE Transactions on Nuclear Science, 1996. **43**(2): p. 561-575.
2. Horn, K.M., B.L. Doyle, and F.W. Sexton, *Nuclear Microprobe Imaging of Single-Event Upsets.* IEEE Transactions on Nuclear Science, 1992. **39**(1): p. 7-12.
3. Oikawa, M., et al., *Design of a focusing high-energy heavy ion microbeam system at the JAERI AVF cyclotron.* Nuclear Instruments & Methods in Physics Research Section B-Beam Interactions with Materials and Atoms, 2003. **210**: p. 54-58.
4. Oikawa, M., et al., *Focusing high-energy heavy ion microbeam system at the JAEA AVF cyclotron.* Nuclear Instruments & Methods in Physics Research Section B-Beam Interactions with Materials and Atoms, 2007. **260**(1): p. 85-90.
5. Doyle, B.L., et al., *Nuclear emission microscopies.* Nuclear Instruments & Methods in Physics Research Section B-Beam Interactions with Materials and Atoms, 2001. **181**: p. 199-210.
6. Doyle, B.L., et al., *A new approach to nuclear microscopy: the ion-electron emission microscope.* Nuclear Instruments & Methods in Physics Research Section B-Beam Interactions with Materials and Atoms, 1999. **158**(1-4): p. 6-17.
7. Doyle, B.L., et al., *Axial ion-electron emission microscopy of IC radiation hardness.* Nuclear Instruments & Methods in Physics Research Section B-Beam Interactions with Materials and Atoms, 2002. **190**: p. 19-25.
8. Doyle, B.L., et al., *Logic upsets in SRAMs using ion electron emission microscopy.* Nuclear Instruments & Methods in Physics Research Section B-Beam Interactions with Materials and Atoms, 2003. **210**: p. 98-103.
9. Bisello, D., et al. *Status of the ion electron emission microscope at the SIRAD single event effect facility*. in *8th International Conference on Nuclear Microprobe Technology and Applications*. 2002. Takasaki Gunma, Japan.
10. Bisello, D., et al. *Ion electron emission microscopy at SIRAD*. in *9th International Conference on Nuclear Microprobe Technology and Applications*. 2004. Cavtat, CROATIA.
11. Bisello, D., et al. *Detection efficiency and spatial resolution of the SIRAD ion electron emission microscope*. in *11th International Conference on Nuclear Microprobe Technology and Applications/3rd International Workshop on Proton Beam Writing*. 2008. Debrecen, HUNGARY.
12. Bisello, D., et al. *Performance of the SIRAD ion electron emission microscope*. in *9th European Conference on Accelerators in Applied Research and Technology*. 2007. Florence, ITALY.
13. Wyss, J., et al. *The future of the SIRAD SEE facility: Ion-electron emission microscopy*. in *3rd International Conference on Radiation Effects on Semiconductor Materials, Detectors and Devices*. 2000. Florence, Italy.
14. Rossi, P., et al., *Phosphors' lifetime measurement employing the Time Between Photons method.* Nuclear Instruments & Methods in Physics Research Section B-Beam Interactions with Materials and Atoms, 2009. **267**: p. 2193-2196.
15. Vij, D.R. "Theory of Luminescence" and "Ionoluminescence". *Luminescence of Solids*. New York. 1998. p. 1-40 and 189-218.

16. Leroy, C. and Rancoita, P-G. "Electromagnetic Interaction of Radiation in Matter" and "Scintillating Media and Scintillator Detectors". *Principles of Radiation Interaction in Matter and Detection.* New Jersey. 2004. p. 27-68 and 291-299.
17. Malmqvist, K.G., *Ion Beam Induced Luminescence*. Solid State Phenomena, 1998. **63-64:** p. 147-150.
18. *The Ionoluminescence Method*. University of Leipzig. *Online.* http://www.uni-leipzig.de/~nfp/Research/Methods/Ion_Beam_Analysis/IL/body_il.html

DISTRIBUTION

4 Lawrence Berkeley National Laboratory
Attn: L. W. Phair
1 Cyclotron Road Mail Stop 88R0192
Berkeley, CA 94720

1	MS0260	Frederick W. Sexton	048471
1	MS1056	Barney L. Doyle	01111
1	MS1056	James A. Knapp	01111
1	MS1056	Gyorgy Vizkelethy	01111
1	MS1083	Paul E. Dodd	017311
1	MS1083	James R. Schwank	017311
1	MS1083	Marty R. Shaneyfelt	017311
1	MS1167	Frederick E. Hartman	01343
1	MS1169	James R. Lee	01300
1	MS1415	Paolo Rossi	01111
1	MS1423	Janelle V. Branson	01111
1	MS1423	Khalid M. Hattar	01111

2	MS9018	Central Technical Files	8944
1	MS0899	Technical Library	9536 (electronic copy)

1	MS0123	D. Chavez, LDRD Office	1011


Sandia National Laboratories